

An explicit solution for inelastic buckling of rectangular plates subjected to combined biaxial and shear loads

Alireza Jahanpour¹, Reijo Kouhia²

1- Corresponding Author, Department of Civil Engineering, Malayer University, Malayer, Iran

Tel: +988132233113, Fax: +988132221977

Email: a.jahanpour@malayeru.ac.ir

ORCID: 0000-0001-9873-8086

2- Department of Structural Engineering, Tampere University, Tampere, Finland

Abstract

In this study, the inelastic buckling equation of thin plate subjected to all in-plane loads is analytically solved and the inelastic buckling coefficient is explicitly estimated. Using the deformation theory of plasticity, a multiaxial nonlinear stress-strain curve is supposed which is described by Ramberg-Osgood representation and von-Mises criterion. Due to buckling, the variations are applied on the secant modulus, the Poisson's ratio and normal and shear strains. Then, inelastic buckling equation of perfect thin rectangular plate subjected to combined biaxial and shear loads is completely developed. Applying the generalized integral transform technique (GITT), the equation is straightforwardly converted to an eigenvalue problem in a dimensionless form. Initially, a geometrical solution and an algorithm are presented to find the lowest inelastic buckling coefficient (k_s). The solution is successfully validated by some results in the literature. Then, a semi-analytical solution is proposed to simplify the calculation of k_s . The method of linear least squares (LLS) is applied in two stages on the obtained results and an approximate polynomial equation is found which is usually solved by trial and error method. The obtained results show good agreement between the proposed semi-analytical and geometrical methods, so that the differences are less than 12%. The semi-analytical solution is easily programmed in the usual scientific calculators and can be applied for the practical purposes.

Keywords: Deformation theory of plasticity; Inelastic buckling of plate; Biaxial and shear loads; Ramberg-Osgood representation; Generalized integral transform technique; Eigenvalue problem.

1 Introduction

The stability of structural plates is one of the most important design criteria in mechanics, civil, aerospace and marine engineering. During their lifetime, various loads are applied on them to perform in-plane stresses on their edges. In addition to shear stress, the edges may experience compressive or tensile (biaxial) stresses and due to the geometrical and material properties of plate, inelastic buckling may occur. An analytical procedure may be quite complicated for solution of the inelastic buckling equation of plate with diverse boundary conditions and under multiaxial loadings. Thus, an explicit solution should be preferably developed using the theories of plasticity to predict the inelastic buckling load of plates.

In the 1940s, two main plasticity models were applied to describe the inelastic buckling of plates. Ilyushin [1], Stowell [2] and Bijlaard [3] used the deformation (total) theory of plasticity while Handelman and Prager [4] used the incremental (flow) theory of plasticity. In the deformation theory of plasticity, the total strain is related to the total stress by the secant modulus without any consideration of stress history and then, the surveyed path to get a particular point on the stress-strain curve is not definitely important. As only the secant modulus appears in the stress-strain relations, the hardening is isotropic in this theory. Nevertheless, in the incremental theory of plasticity, the stress at any point and time is a function of the current strain as well as the history of strain. In other words, increments of strain are related to increments of stress by the tangent modulus which lead to a complicated nonlinear stress-strain relation. Applying the variational approach on the stress-strain relations, only the tangent modulus appears in the incremental theory while both the secant and tangent modulus appear in the deformation theory. Generally, the not very complicated deformation theory relations are comparable with very complicated incremental theory relations for inelastic stress analysis. Although the incremental theory of plasticity is more general than the deformation theory, the latter one can be successfully applicable to the proportional loading problems in which the components of stress tensor increase in constant ratio to each other [5, 6]. In addition, the deformation theory is an acceptable approach for the bifurcation check in the buckling of plates and provides good agreement with measured buckling loads for bars, plates and shells, while the incremental theory predicts much higher than the measured buckling loads [7]. This discrepancy which is called '*plastic buckling paradox*' [7], has not generally solved until recent times [8]. One of the oldest problems which directly refers to this '*paradox*' and reported in the literature, is the inelastic stability of cruciform columns [7, 9-11]. Recently, Guarracino and Simonelli [12] showed that the torsional buckling of a cruciform column in the inelastic range is not actually '*plastic buckling paradox*' if effects of the imperfections are accurately computed up to the limit load. Their analytical procedure represented very good agreement between flow and deformation theories for this problem. The '*plastic buckling paradox*' was also tried to solve for circular cylindrical shells under both axial and non-proportional loading [13, 14]. The results of finite element analysis were compared with those of the experimental studies and concluded that the adaptation of flow theory of plasticity with the experimental findings depends on the assuming of initial imperfections and buckling shapes.

Shamass [15] reviewed in detail many aspects which are effect on the '*plastic buckling paradox*'. In this review, the considered aspects are the effective shear modulus, initial imperfections, different material constitutive models, transverse shear deformation, deformations in the pre-bifurcation state, actual boundary conditions, sensitivity of the

predictions by different plasticity theories and effect of the kinematic constraints used in analytical treatments. It is concluded that the incremental theory does not have any limitation and a number of combined approximations effect on the results predicted by the incremental theory.

Generally, the variations of strains and stresses during buckling are used to develop inelastic buckling equation of plates. In the initial studies of deformation theory of plasticity, the material was supposed to be incompressible in the nonlinear (elastoplastic) region of stress-strain curve and then, the Poisson's ratio was always $\frac{1}{2}$ for isotropic materials. As a result, the variation was being only applied on the strains and secant modulus in the stress-strain relations (Hooke's law) as seen in the approaches of Ilyushin [1] and Stowell [2]. Pifko and Isakson [16], Bradford and Azhari [17], Ibearugbulem, et al. [18, 19], Onwuka, et al. [20] and Eziefula, et al. [21] applied Stowell's procedure in their studies. However, in several investigations [22-35], Bijlaard's formulation [3] has been applied in which the Poisson's ratio appears in the elastic value during the inelastic buckling. Gerard and Wildhorn [36] showed that for a nonlinear stress-strain curve such as Ramberg-Osgood representation [37], the Poisson's ratio changes from the elastic value to the incompressible value of $\frac{1}{2}$ as the stress is increased above the yield stress,

$$\nu = \frac{1}{2} - \frac{E_{sec}}{E} \left(\frac{1}{2} - \nu_e \right) \quad (1)$$

where E is the Young's modulus (or the slop of stress-strain curve at zero stress), E_{sec} is the secant modulus and ν_e is the elastic Poisson's ratio. Using Eq. (1), the variable Poisson's ratio is considered in the elastoplastic region of stress-strain curve as well as the other parameters [38-43]. Jones [6] successfully applied variation to the Poisson's ratio and developed the inelastic buckling equation of plate subjected to biaxial loads, although the obtained equation was only solved for the uniaxial loading.

The elastic / Inelastic buckling of plates is analytically formulated with a fourth order linear partial differential equation. In recent decades, several numerical and semi-analytical methods have been proposed to solve this equation with different boundary conditions and mostly uniaxial loading. The most important of these methods are finite element (FE) [16, 44, 45], finite difference [42], finite strip [31], spline finite strip [24], isoparametric spline finite strip [29, 46], complex finite strip [17, 26, 47], finite layer (FL) [48], differential quadrature (DQ) [30, 43], generalized differential quadrature (GDQ) [33-35], element-free Galerkin (EFG) [32], funicular polygon (FP) [23], p-Ritz [49, 50], Rayleigh-Ritz [51-53], and virtual work principle [18-21]. [The integral transforms have been already used for solving complex boundary value problems in elastic bending, buckling and vibration of beams. Fourier series were](#)

differentiated as many as four times to solve the corresponding ordinary differential equations. In 1944, Green [54] extended double Fourier series for solving elastic problems of isotropic rectangular plates in which partial differential equations appear. Later, this method was used for the buckling of simply supported orthotropic and isotropic skew plates, subjected to in-plane compressive and shear edge loads [55]. Afterward, double finite integral transform and the corresponding inversion formula were analytically used to solve the bending equation of rectangular thin / thick plates with different boundary conditions [56-60]. As double finite integral transform has some restrictions for complex boundary conditions, it may be modified to the generalized integral transform technique (GITT) which is mathematically more general with faster convergence. This technique was previously applied in the automatic and accuracy-controlled solution of nonlinear diffusion and convection-diffusion problems as well as solution of Navier-Stokes equations [61]. In the GITT, an appropriate auxiliary eigenvalue problem is solved to find the kernel of integral transform. Then, applying the integral transformation to an ordinary / a partial differential equation, it is transformed into infinite algebraic / ordinary differential equations and then, they are truncated at finite terms to allow the computational solution. Alternatively, double integral transformation can be directly applied to a PDE for obtaining the infinite algebraic equations. For bending, buckling and vibration problems of rectangular plates, the kernels of double integral transform are similar to the vibrating functions of two beams which have the same material properties and boundary conditions of plates in two orthogonal directions. If the original PDE is linear, then the linear algebraic equations are naturally obtained, so that they can be analytically solved for the bending problem and on the other hand, lead to an eigenvalue problem for buckling / vibration of plate. Thus, the buckling load / natural frequency is obtained for each mode as well as the corresponding mode shape. An et al. [62] used the GITT as single integral transform, so that the original PDE is transformed into a set of coupled ordinary differential equations. Furthermore, Ullah et al. [63] employed the GITT and solved an eigenvalue problem to obtain the elastic buckling coefficient of uniaxial loaded fully clamped plates (CCCC), plates with three clamped and one edge simply supported (CCCS), and plates with two adjacent edges clamped and the other edges simply supported (CCSS). The GITT has been also applied for the bending solution of orthotropic rectangular thin foundation plates [64] as well as free vibration of orthotropic rectangular plates with free edges [65].

In this study, using the deformation theory of plasticity [6] and applying variations to all mechanical components of an isotropic perfect rectangular plate, the complete equation of inelastic buckling of plates under combined biaxial and shear stresses is developed. The parameters of Ramberg-Osgood representation are used to find the secant and

tangent moduli in the nonlinear region of stress-strain curve. Then, using the generalized integral transform technique (GITT) [62-65], the inelastic buckling equation is solved for simply supported (SSSS) and fully clamped (CCCC) plates and the effect of variation of Poisson's ratio on the inelastic buckling load is compared with those of previous studies. The rectangular plate may be subjected to compressive-compressive-shear (CCS), compressive-tensile-shear (CTS), tensile-compressive-shear (TCS) or tensile-tensile-shear (TTS) loads. A geometrical solution and an algorithm are presented to find the inelastic buckling coefficient of plate based on the aspect ratio, thickness ratio, load ratios, secant to Young's modules ratio, elastic Poisson's ratio and Ramberg-Osgood parameters. Using the obtained results and linear regression technique (linear least squares), a semi-analytical procedure is also suggested to calculate the lowest inelastic buckling coefficient. In this procedure, a q^{th} order equation must be solved using trial and error method in which q is the shape parameter of Ramberg-Osgood representation. The procedure is applicable in the practical purposes and can be easily programed in usual scientific calculators.

2 Analytical approach

2.1 Inelastic buckling equation of plate

Consider a rectangular plate with dimensions of $a \times b \times t$ subjected to CCS, CTS, TCS or TTS loads in the shown Cartesian coordinate system in Figure 1. In this Figure, $N_x = t\sigma_x$, $N_y = t\sigma_y$ and $N_{xy} = t\tau$ are the applied loads per unit length on the plate edges in x -, y - and xy - directions respectively. Also, σ_x , σ_y and τ are the stresses in x -, y - and xy - directions respectively.

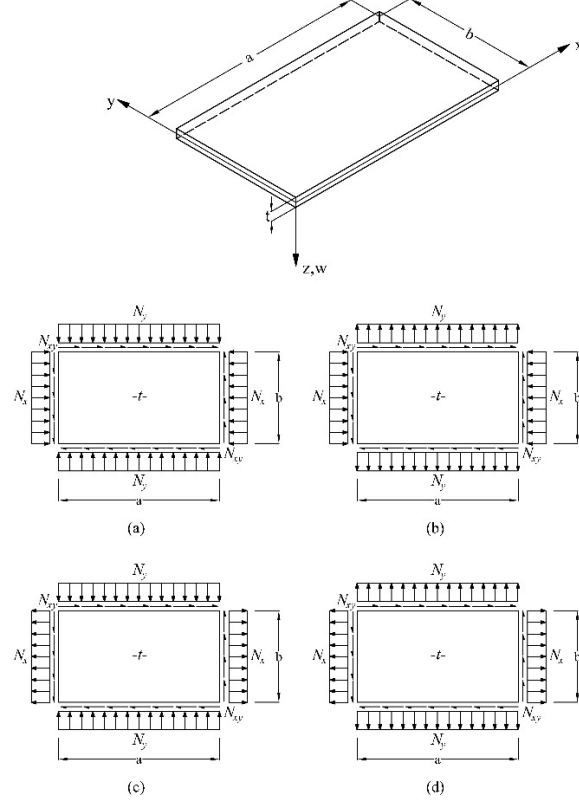


Fig. 1 A rectangular plate subjected to (a) CCS, (b) CTS, (c) TCS and (d) TTS loads

In the deformation theory of plasticity, using general nonlinear materials properties (E_{sec} and ν), the two-dimensional stress-strain relations are established as shown in Eq. 2. In these relations, ε_x , ε_y and γ are the strains in x -, y - and xy -directions respectively and ν is obtained from Eq. (1).

$$\begin{bmatrix} \sigma_x \\ \sigma_y \\ \tau \end{bmatrix} = \frac{E_{sec}}{1 - \nu^2} \begin{bmatrix} 1 & \nu & 0 \\ \nu & 1 & 0 \\ 0 & 0 & \frac{1 - \nu}{2} \end{bmatrix} \begin{bmatrix} \varepsilon_x \\ \varepsilon_y \\ \gamma \end{bmatrix} \quad (2)$$

After applying the variations to all components of Eq. (2),

$$\begin{bmatrix} \delta\sigma_x \\ \delta\sigma_y \\ \delta\tau \end{bmatrix} = \frac{E_{sec}}{1 - \nu^2} \begin{bmatrix} D_{11} & D_{12} & D_{13} \\ D_{12} & D_{22} & D_{23} \\ D_{13} & D_{23} & D_{33} \end{bmatrix} \begin{bmatrix} \delta\varepsilon_{0x} + z\delta k_x \\ \delta\varepsilon_{y0} + z\delta k_y \\ \delta\gamma_0 + z\delta k_{xy} \end{bmatrix} \quad (3)$$

where $\delta\varepsilon_{0x}$, $\delta\varepsilon_{y0}$ and $\delta\gamma_0$ are the variations of middle surface strains in x-, y- and xy- directions respectively, $\delta\kappa_x = -\frac{\partial^2\delta w}{\partial x^2}$, $\delta\kappa_y = -\frac{\partial^2\delta w}{\partial y^2}$ are the variation of curvatures in x- and y- directions respectively, $\delta\kappa_{xy} = -2\frac{\partial^2\delta w}{\partial x\partial y}$ is the variation of twist and z is the distance from the middle surface of plate as shown in Figure 1. In addition,

$$\begin{aligned}
D_{11} &= 1 - \frac{\bar{K}}{4(1-\nu^2)} [(2-\nu)\sigma_x - (1-2\nu)\sigma_y]^2 \\
D_{12} &= \nu - \frac{\bar{K}}{4(1-\nu^2)} [(2-\nu)\sigma_x - (1-2\nu)\sigma_y][(2-\nu)\sigma_y - (1-2\nu)\sigma_x] \\
D_{13} &= -\frac{3\bar{K}\tau}{4(1+\nu)} [(2-\nu)\sigma_x - (1-2\nu)\sigma_y] \\
D_{22} &= 1 - \frac{\bar{K}}{4(1-\nu^2)} [(2-\nu)\sigma_y - (1-2\nu)\sigma_x]^2 \\
D_{23} &= -\frac{3\bar{K}\tau}{4(1+\nu)} [(2-\nu)\sigma_y - (1-2\nu)\sigma_x] \\
D_{33} &= \frac{1-\nu}{2} \left[1 - \frac{9\bar{K}\tau^2}{2(1+\nu)} \right]
\end{aligned} \tag{4}$$

In Eqs. (4), $\bar{K} = \frac{1}{\sigma_i^2 \bar{H}} \left(1 - \frac{E_{tan}}{E_{sec}} \right)$ where $\sigma_i = \sqrt{\sigma_x^2 - \sigma_x\sigma_y + \sigma_y^2 + 3\tau^2}$ is the stress intensity based on von-Mises criteria and E_{tan} is the tangent modulus. Also,

$$\bar{H} = 1 - \frac{1-2\nu}{2(1-\nu^2)} \frac{E_{sec}}{E} \left(1 - \frac{E_{tan}}{E_{sec}} \right) \left[2\nu - \frac{(1+2\nu)(\sigma_x^2 + \sigma_y^2) - 2(2+\nu)\sigma_x\sigma_y + 6(1+\nu)\tau^2}{2\sigma_i^2} \right] \tag{5}$$

Substituting Eq. (3) into Eq. (6), the moment-curvature relations can be determined (Eq. 7).

$$\begin{bmatrix} \delta M_x \\ \delta M_y \\ \delta M_{xy} \end{bmatrix} = \int_{-\frac{t}{2}}^{\frac{t}{2}} \begin{bmatrix} \delta\sigma_x \\ \delta\sigma_y \\ \delta\tau \end{bmatrix} z dz \tag{6}$$

$$\begin{bmatrix} \delta M_x \\ \delta M_y \\ \delta M_{xy} \end{bmatrix} = \frac{E_{sec}t^3}{12(1-\nu^2)} \begin{bmatrix} D_{11} & D_{12} & D_{13} \\ D_{12} & D_{22} & D_{23} \\ D_{13} & D_{23} & D_{33} \end{bmatrix} \begin{bmatrix} \delta\kappa_x \\ \delta\kappa_y \\ \delta\kappa_{xy} \end{bmatrix} \tag{7}$$

Substituting Eq. (7) into the equilibrium equation,

$$\frac{\partial^2(\delta M_x)}{\partial x^2} + \frac{\partial^2(\delta M_{xy})}{\partial x\partial y} + \frac{\partial^2(\delta M_y)}{\partial y^2} = N_x \frac{\partial^2(\delta w)}{\partial x^2} + 2N_{xy} \frac{\partial^2(\delta w)}{\partial x\partial y} + N_y \frac{\partial^2(\delta w)}{\partial y^2}$$

the inelastic buckling equation of plate will be obtained:

$$\begin{aligned}
& D_{11} \frac{\partial^4(\delta w)}{\partial x^4} + 4D_{13} \frac{\partial^4(\delta w)}{\partial x^3 \partial y} + 2(D_{12} + 2D_{33}) \frac{\partial^4(\delta w)}{\partial x^2 \partial y^2} + 4D_{23} \frac{\partial^4(\delta w)}{\partial x \partial y^3} + D_{22} \frac{\partial^4(\delta w)}{\partial y^4} \\
& + \frac{12(1 - \nu^2)}{E_{sec} t^3} \left[N_x \frac{\partial^2(\delta w)}{\partial x^2} + 2N_{xy} \frac{\partial^2(\delta w)}{\partial x \partial y} + N_y \frac{\partial^2(\delta w)}{\partial y^2} \right] = 0
\end{aligned} \tag{8}$$

2.2 Generalized integral transform technique (GITT)

When the GITT is used for a two-dimensional boundary value problem, two appropriate auxiliary ODEs must be solved. Here, they are the vibrating beam equations (Eqs. 9) which satisfy the corresponding boundary conditions (Eqs. 10 and 11) and orthogonality (Eqs. 12 and 13) in x - and y - directions:

$$\begin{cases} \frac{d^4 X_m(x)}{dx^4} = \alpha_m^4 X_m(x) \\ \frac{d^4 Y_n(y)}{dy^4} = \beta_n^4 Y_n(y) \end{cases} \tag{9}$$

$$\begin{aligned}
x = 0, a \rightarrow & \left\{ \begin{array}{l} X_m(x) = 0 \\ \frac{d^2 X_m(x)}{dx^2} = 0 \end{array} \right\}; SS \\
y = 0, b \rightarrow & \left\{ \begin{array}{l} Y_n(y) = 0 \\ \frac{d^2 Y_n(y)}{dy^2} = 0 \end{array} \right\}
\end{aligned} \tag{10}$$

$$\begin{aligned}
x = 0, a \rightarrow & \left\{ \begin{array}{l} X_m(x) = 0 \\ \frac{dX_m(x)}{dx} = 0 \end{array} \right\}; CC \\
y = 0, b \rightarrow & \left\{ \begin{array}{l} Y_n(y) = 0 \\ \frac{dY_n(y)}{dy} = 0 \end{array} \right\}
\end{aligned} \tag{11}$$

$$\begin{aligned}
\int_0^a X_m(x) X_r(x) dx &= \begin{cases} \frac{a}{2} & m = r \\ 0 & m \neq r \end{cases} \\
\int_0^b Y_n(y) Y_s(y) dy &= \begin{cases} \frac{b}{2} & n = s \\ 0 & n \neq s \end{cases}
\end{aligned} \tag{12}$$

$$\begin{aligned}
\int_0^a X_m(x) X_r(x) dx &= \begin{cases} a & m = r \\ 0 & m \neq r \end{cases} \\
\int_0^b Y_n(y) Y_s(y) dy &= \begin{cases} b & n = s \\ 0 & n \neq s \end{cases}
\end{aligned} \tag{13}$$

where SS and CC are used for simply supported and clamped beams respectively and m, n, r and s are positive integers.

Eqs. (9) are readily solved for the different boundary conditions (Eqs. 10 and 11) to yield the related eigenfunctions

which are shown in Eqs. (14) and (15) for SS and CC beams respectively:

$$\begin{cases} X_m(x) = \sin \alpha_m x \\ Y_n(y) = \sin \beta_n y \end{cases} \quad (14)$$

$$\begin{cases} X_m(x) = \cosh \alpha_m x - \cos \alpha_m x - c_m(\sinh \alpha_m x - \sin \alpha_m x) \\ Y_n(y) = \cosh \beta_n y - \cos \beta_n y - c_n(\sinh \beta_n y - \sin \beta_n y) \end{cases} \quad (15)$$

where

$$\begin{cases} c_m = \frac{\cosh \alpha_m a - \cos \alpha_m a}{\sinh \alpha_m a - \sin \alpha_m a} \\ c_n = \frac{\cosh \beta_n b - \cos \beta_n b}{\sinh \beta_n b - \sin \beta_n b} \end{cases} \quad (16)$$

In Eqs. (14) and (15), α_m and β_n are the roots of transcendental beam frequency equations:

$$\begin{cases} \sin \alpha_m a \cdot \sinh \alpha_m a = 0 \Rightarrow \alpha_m a = m\pi \\ \sin \beta_n b \cdot \sinh \beta_n b = 0 \Rightarrow \beta_n b = n\pi \end{cases}; SSSS \quad (17)$$

$$\begin{cases} \cosh \alpha_m a \cdot \cos \alpha_m a = 1 \Rightarrow \alpha_m a \cong \left[(2m+1)\frac{\pi}{2} + 2(-1)^{m+1}e^{-(2m+1)\frac{\pi}{2}} \right] \\ \cosh \beta_n b \cdot \cos \beta_n b = 1 \Rightarrow \beta_n b \cong \left[(2n+1)\frac{\pi}{2} + 2(-1)^{n+1}e^{-(2n+1)\frac{\pi}{2}} \right] \end{cases}; CCCC \quad (18)$$

Using the obtained eigenfunctions in Eqs (14 and 15), two-dimensional generalized finite integral transform and the corresponding inversion are defined as:

$$\delta w_{mn} = \int_0^a \int_0^b \delta w(x, y) X_m(x) Y_n(y) dx dy \quad (19)$$

$$\delta w(x, y) = \frac{1}{\mu \phi b^2} \sum_{m=1}^{\infty} \sum_{n=1}^{\infty} \delta w_{mn} X_m(x) Y_n(y) \quad (20)$$

where

$$\mu = \frac{1}{\phi b^2} \int_0^a X_m^2(x) dx \cdot \int_0^b Y_n^2(y) dy = \begin{cases} \frac{1}{4} & ; SSSS \\ 1 & ; CCCC \end{cases} \quad (21)$$

and $\phi = \frac{a}{b}$ is the plate aspect ratio.

2.3 Analytical procedure for inelastic buckling

The GITT should be applied on all terms of Eq. (8). Using integration by parts in the successive steps, fourth and second orders partial derivatives in Eq. (8) are reduced and finally, $\delta w(x, y)$ is transformed to δw_{mn} based on Eq.

(19). In Eqs. (22)-(29), these transformations are shown with the dimensionless coefficients.

$$b^4 \int_0^a \int_0^b \frac{\partial^4(\delta w)}{\partial x^4} X_m(x) Y_n(y) dx dy = \left(\frac{\alpha_m a}{\phi} \right)^4 \delta w_{mn} \quad (22)$$

$$b^4 \int_0^a \int_0^b \frac{\partial^4(\delta w)}{\partial x^3 \partial y} X_m(x) Y_n(y) dx dy = \frac{1}{\mu \phi^3} \sum_{r=1}^{\infty} \sum_{s=1}^{\infty} \delta w_{rs} [(B_{mr} a^2) + (J_{mr} a^2)] L_{ns} \quad (23)$$

$$b^4 \int_0^a \int_0^b \frac{\partial^4(\delta w)}{\partial x^2 \partial y^2} X_m(x) Y_n(y) dx dy = \frac{1}{\mu \phi^2} \sum_{r=1}^{\infty} \sum_{s=1}^{\infty} \delta w_{rs} (I_{mr} a) (P_{ns} b) \quad (24)$$

$$b^4 \int_0^a \int_0^b \frac{\partial^4(\delta w)}{\partial x \partial y^3} X_m(x) Y_n(y) dx dy = \frac{1}{\mu \phi} \sum_{r=1}^{\infty} \sum_{s=1}^{\infty} \delta w_{rs} [(F_{ns} b^2) + (Q_{ns} b^2)] H_{mr} \quad (25)$$

$$b^4 \int_0^a \int_0^b \frac{\partial^4(\delta w)}{\partial y^4} X_m(x) Y_n(y) dx dy = (\beta_n b)^4 \delta w_{mn} \quad (26)$$

$$b^2 \int_0^a \int_0^b \frac{\partial^2(\delta w)}{\partial x^2} X_m(x) Y_n(y) dx dy = \frac{1}{\mu \phi^2} \sum_{r=1}^{\infty} \sum_{s=1}^{\infty} \delta w_{rs} (I_{mr} a) \left(\frac{K_{ns}}{b} \right) \quad (27)$$

$$b^2 \int_0^a \int_0^b \frac{\partial^2(\delta w)}{\partial x \partial y} X_m(x) Y_n(y) dx dy = \frac{1}{\mu \phi} \sum_{r=1}^{\infty} \sum_{s=1}^{\infty} \delta w_{rs} H_{mr} L_{ns} \quad (28)$$

$$b^2 \int_0^a \int_0^b \frac{\partial^2(\delta w)}{\partial y^2} X_m(x) Y_n(y) dx dy = \frac{1}{\mu} \sum_{r=1}^{\infty} \sum_{s=1}^{\infty} \delta w_{rs} \left(\frac{G_{mr}}{a} \right) (P_{ns} b) \quad (29)$$

where

$$a^2 B_{mr} = a^2 \left(\frac{dX_r}{dx} \Big|_{x=a} \cdot \frac{dX_m}{dx} \Big|_{x=a} - \frac{dX_r}{dx} \Big|_{x=0} \cdot \frac{dX_m}{dx} \Big|_{x=0} \right) = \begin{cases} -[1 - (-1)^{m+r}] mr \pi^2; & SS \\ 0 & ; CC \end{cases} \quad (30)$$

$$\frac{G_{mr}}{a} = \frac{1}{a} \int_0^a X_r(x) X_m(x) dx = \begin{cases} \left\{ \frac{1}{2} \ ; \ m = r \right\}; & SS \\ 0 \ ; \ m \neq r \end{cases} \quad (31)$$

$$H_{mr} = \int_0^a X_r(x) \frac{dX_m(x)}{dx} dx = \begin{cases} \begin{cases} \frac{2mr}{r^2 - m^2} & ; m \pm r = \text{odd} \\ 0 & ; m \pm r = \text{even} \end{cases} ; SS \\ \begin{cases} 0 & ; m = r \\ \frac{4(\alpha_m a)^2 (\alpha_r a)^2}{(\alpha_r a)^4 - (\alpha_m a)^4} [1 - (-1)^{m+r}] & ; m \neq r \end{cases} ; CC \end{cases} \quad (32)$$

$$aI_{mr} = a \int_0^a X_r(x) \frac{d^2 X_m(x)}{dx^2} dx = \begin{cases} \begin{cases} -\frac{m^2 \pi^2}{2} & ; m = r \\ 0 & ; m \neq r \end{cases} ; SS \\ \begin{cases} c_m(\alpha_m a)[2 - c_m(\alpha_m a)] & ; m = r \\ \frac{4(\alpha_m a)^2 (\alpha_r a)^2}{(\alpha_m a)^4 - (\alpha_r a)^4} [c_m(\alpha_m a) - c_r(\alpha_r a)][1 + (-1)^{m+r}] & ; m \neq r \end{cases} ; CC \end{cases} \quad (33)$$

$$a^2 J_{mr} = a^2 \int_0^a X_r(x) \frac{d^3 X_m(x)}{dx^3} dx = \begin{cases} \begin{cases} \frac{2m^3 r \pi^2}{m^2 - r^2} & ; m \pm r = \text{odd} \\ 0 & ; m \pm r = \text{even} \end{cases} ; SS \\ \begin{cases} 0 & ; m = r \\ \frac{4(\alpha_m a)^3 (\alpha_r a)^3}{(\alpha_m a)^4 - (\alpha_r a)^4} c_m c_r [1 - (-1)^{m+r}] & ; m \neq r \end{cases} ; CC \end{cases} \quad (34)$$

$$b^2 F_{ns} = b^2 \left(\frac{dY_s}{dy} \Big|_{y=b} \cdot \frac{dY_n}{dy} \Big|_{y=b} - \frac{dY_s}{dy} \Big|_{y=0} \cdot \frac{dY_n}{dy} \Big|_{y=0} \right) = \begin{cases} -[1 - (-1)^{n+s}] ns \pi^2 ; SS \\ 0 ; CC \end{cases} \quad (35)$$

$$\frac{K_{ns}}{b} = \frac{1}{b} \int_0^b Y_s(y) Y_n(y) dy = \begin{cases} \begin{cases} \frac{1}{2} & ; n = s \\ 0 & ; n \neq s \end{cases} ; SS \\ \begin{cases} 1 & ; n = s \\ 0 & ; n \neq s \end{cases} ; CC \end{cases} \quad (36)$$

$$L_{ns} = \int_0^b Y_s(y) \frac{dY_n(y)}{dx} dy = \begin{cases} \begin{cases} \frac{2ns}{s^2 - n^2} & ; n \pm s = \text{odd} \\ 0 & ; n \pm s = \text{even} \end{cases} ; SS \\ \begin{cases} 0 & ; n = s \\ \frac{4(\beta_n b)^2 (\beta_s b)^2}{(\beta_s b)^4 - (\beta_n b)^4} [1 - (-1)^{n+s}] & ; n \neq s \end{cases} ; CC \end{cases} \quad (37)$$

$$bP_{ns} = b \int_0^b Y_s(y) \frac{d^2 Y_n(y)}{dy^2} dy = \begin{cases} \begin{cases} -\frac{n^2 \pi^2}{2} & ; n = s \\ 0 & ; n \neq s \end{cases} & ; SS \\ \begin{cases} c_n(\beta_n b)[2 - c_n(\beta_n b)] & ; n = s \\ \frac{4(\beta_n b)^2(\beta_s b)^2}{(\beta_n b)^4 - (\beta_s b)^4} [c_n(\beta_n b) - c_s(\beta_s b)][1 + (-1)^{n+s}] & ; n \neq s \end{cases} & ; CC \end{cases} \quad (38)$$

$$b^2 Q_{ns} = b^2 \int_0^b Y_s(y) \frac{d^3 Y_n(y)}{dy^3} dy = \begin{cases} \begin{cases} \frac{2n^3 s \pi^2}{n^2 - s^2} & ; n \pm s = odd \\ 0 & ; n \pm s = even \end{cases} & ; SS \\ \begin{cases} 0 & ; n = s \\ \frac{4(\beta_n b)^3(\beta_s b)^3}{(\beta_n b)^4 - (\beta_s b)^4} c_n c_s [1 - (-1)^{n+s}] & ; n \neq s \end{cases} & ; CC \end{cases} \quad (39)$$

Applying the GITT into Eq. (8) and using Eqs. (22)-(29), the characteristic equation in dimensionless form will be obtained:

$$\begin{aligned} & \left[\left(\frac{\alpha_m a}{\phi} \right)^4 D_{11} + (\beta_n b)^4 D_{22} \right] \delta w_{mn} \\ & + \frac{1}{\mu \phi} \sum_{r=1}^{\infty} \sum_{s=1}^{\infty} \delta w_{rs} \left\{ \frac{4}{\phi^2} D_{13} [(a^2 B_{mr}) + (a^2 J_{mr})] L_{ns} + \frac{2}{\phi} (D_{12} + 2D_{33}) (a I_{mr}) (b P_{ns}) \right. \\ & + 4D_{23} [(b^2 F_{ns}) + (b^2 Q_{ns})] H_{mr} \\ & \left. + \frac{E(1-\nu^2)}{E_{sec}(1-\nu_e^2)} k_s \pi^2 \left[\frac{\psi_x}{\phi} (a I_{mr}) \left(\frac{K_{ns}}{b} \right) + 2H_{mr} L_{ns} + \phi \psi_y \left(\frac{G_{mr}}{a} \right) (b P_{ns}) \right] \right\} = 0 \end{aligned} \quad (40)$$

where $\psi_x = \frac{N_x}{N_{xy}}$ and $\psi_y = \frac{N_y}{N_{xy}}$ are the load ratios supposing that $N_{xy} \neq 0$ and $k_s = \frac{12(1-\nu_e^2)}{\pi^2} \left(\frac{b}{t} \right)^2 \frac{N_{xy}}{Et}$ is the inelastic buckling coefficient.

Eq. (40) establishes an infinite system of linear equations. For a practical calculation, the positive integers, m , n , r and s must be limited to upper value, h . Thus, Eq. (40) can be shown with a finite number of linear equations in matrix form:

$$\begin{bmatrix} M_{11}^{11} & \cdots & M_{11}^{1h} & \cdots & M_{11}^{h1} & \cdots & M_{11}^{hh} \\ \vdots & \ddots & \vdots & \ddots & \vdots & \ddots & \vdots \\ M_{1h}^{11} & \cdots & M_{1h}^{1h} & \cdots & M_{1h}^{h1} & \cdots & M_{1h}^{hh} \\ \vdots & \ddots & \vdots & \ddots & \vdots & \ddots & \vdots \\ M_{h1}^{11} & \cdots & M_{h1}^{1h} & \cdots & M_{h1}^{h1} & \cdots & M_{h1}^{hh} \\ \vdots & \ddots & \vdots & \ddots & \vdots & \ddots & \vdots \\ M_{hh}^{11} & \cdots & M_{hh}^{1h} & \cdots & M_{hh}^{h1} & \cdots & M_{hh}^{hh} \end{bmatrix} \begin{bmatrix} \delta w_{11} \\ \vdots \\ \delta w_{1h} \\ \vdots \\ \delta w_{h1} \\ \vdots \\ \delta w_{hh} \end{bmatrix} = \begin{bmatrix} 0 \\ \vdots \\ 0 \\ \vdots \\ 0 \\ \vdots \\ 0 \end{bmatrix} \quad (41)$$

where

$$M_{mn}^{rs} = \begin{cases} \left(\frac{\alpha_m a}{\phi} \right)^4 D_{11} + (\beta_n b)^4 D_{22} + T_{mn}^{rs} & ; m = r \text{ and } n = s \\ T_{mn}^{rs} & ; \text{otherwise} \end{cases} \quad (42)$$

and

$$T_{mn}^{rs} = \frac{1}{\mu\phi} \left\{ \frac{4}{\phi^2} D_{13} [(a^2 B_{mr}) + (a^2 J_{mr})] L_{ns} + \frac{2}{\phi} (D_{12} + 2D_{33}) (a I_{mr}) (b P_{ns}) \right. \\ \left. + 4D_{23} [(b^2 F_{ns}) + (b^2 Q_{ns})] H_{mr} \right. \\ \left. + \frac{E(1-\nu^2)}{E_{sec}(1-\nu_e^2)} k_s \pi^2 \left[\frac{\psi_x}{\phi} (a I_{mr}) \left(\frac{K_{ns}}{b} \right) + 2H_{mr} L_{ns} + \phi \psi_y \left(\frac{G_{mr}}{a} \right) (b P_{ns}) \right] \right\} \quad (43)$$

Supposing ψ_x , ψ_y , ν_e , $\frac{E_{sec}}{E}$, $\frac{E_{tan}}{E_{sec}}$, k_s , ϕ and h in Eq. (41), the eigenvalues of coefficient matrix can be calculated for SSSS or CCCC plates. If the smallest eigenvalue is zero, the supposed k_s will be the lowest inelastic critical coefficient ($k_{s,cr}^{(1)} = k_s$). Likewise, if the second, third, or i^{th} eigenvalue is zero, the inelastic critical coefficient is obtained for the corresponding mode. Using the general software python [66] and selecting a few series terms (h) for arrays of coefficient matrix in Eq. (41), the inelastic critical coefficient ($k_{s,cr}$) can be accurately enough obtained for the different buckling modes. However, the secant and tangent moduli relation obviously effects on the inelastic buckling coefficient. For a Ramberg-Osgood stress-strain model, the secant and tangent moduli are defined as [37]:

$$E_{sec} = \frac{E}{1 + \frac{3}{7} \left(\frac{\sigma_i}{\sigma_{.7E}} \right)^{q-1}} \quad (44)$$

$$E_{tan} = \frac{E}{1 + \frac{3q}{7} \left(\frac{\sigma_i}{\sigma_{.7E}} \right)^{q-1}} \quad (45)$$

where $\sigma_{.7E}$ is the stress at which the line with slope $0.7E$ intersects the stress-strain curve and q is a shape parameter which describes the curvature of stress-strain curve. Considering two dimensionless parameters, $\xi = \frac{E_{sec}}{E} \leq 1$ and $\eta =$

$\frac{E_{tan}}{E_{sec}} \leq 1$, Eqs. (44) and (45) may be combined as

$$\eta = \frac{1}{q(1 - \xi) + \xi} \quad (46)$$

so that all terms of arrays of coefficient matrix (Eq. 42) can be expressed by $\phi, \psi_x, \psi_y, \xi, q, v_e$ and k_s . Then using an implicit function, k_s can be briefly described as:

$$k_s = f(\phi, \psi_x, \psi_y, \xi, q, v_e) \quad (47)$$

On the other hand, using Eq. (44), k_s can be expressed with an explicit function:

$$k_s = g\left(\lambda, \frac{E}{\sigma_{.7E}}, \psi_x, \psi_y, \xi, q, v_e\right) = \frac{12(1 - v_e^2)\lambda^2}{\pi^2} \cdot \frac{\sigma_{.7E}}{E} \cdot \frac{\left[\frac{7}{3}\left(\frac{1}{\xi} - 1\right)\right]^{\frac{1}{q-1}}}{(\psi_x^2 - \psi_x\psi_y + \psi_y^2 + 3)^{\frac{1}{2}}} \quad (48)$$

where $\lambda = \frac{b}{t}$ is the plate thickness ratio.

In Eqs. (47) and (48), ξ is a mutual variable in both f and g as well as ψ_x, ψ_y, v_e and q . As ξ is a continuous variable ($0 \leq \xi \leq 1$), both f and g can be plotted in $k_s - \xi$ plane. The intersection of two plotted curves gives the inelastic buckling coefficient as well as the corresponding secant modulus. The described geometrical solution may be summarized by an algorithm as shown in Figure 2. In this algorithm, an initial value of ξ is assumed (ξ_{ini} in Figure 2). In the next steps, ξ is increased by $\delta\xi$ unless $\xi > 1$. In this study, $\xi_{ini} = \delta\xi = 0.025$. In addition, defining a dimensionless parameter, $\Omega = (\psi_x^2 - \psi_x\psi_y + \psi_y^2 + 3)^{\frac{1}{2}}$, Eqs. (4) and (5) are briefly rewritten and finally, the coefficients matrix in Eq. (41) is re-established. In the end of procedure, the $k_s - \xi$ curve will be found for the corresponding buckling mode based on the known parameters: $\phi, \psi_x, \psi_y, v_e$ and q . In this study, the lowest buckling coefficient is calculated. The procedure can be repeated by the new parameters to find new curves.

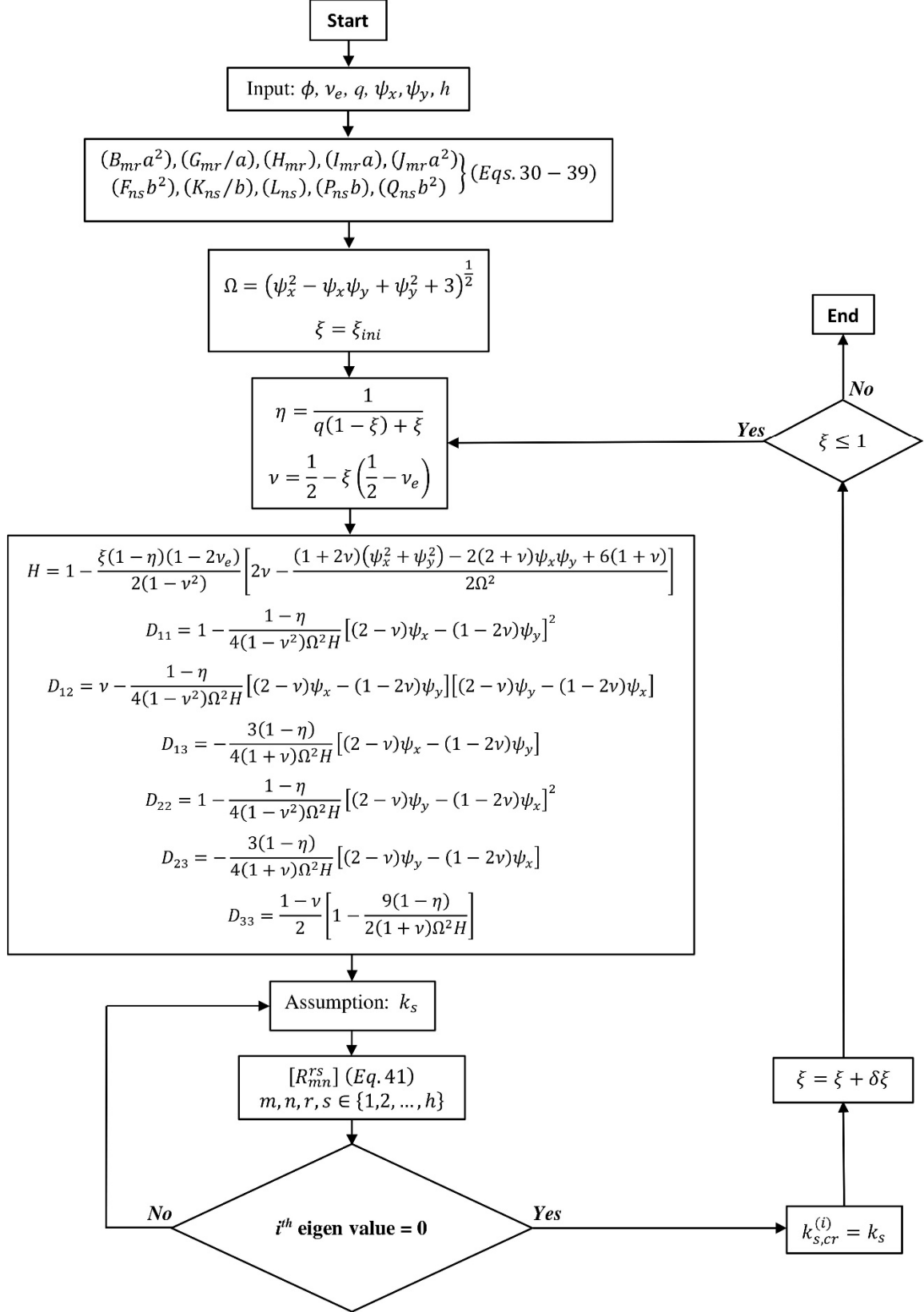


Fig. 2 An algorithm to plot $k_s - \xi$ curve of plate

3 Results and discussion

In this study, the Ramberg-Osgood representation is used for the nonlinear mechanical properties of material, although this approach can be developed for the other known models of nonlinear behavior.

3.1 Validation, effects of variation of Poisson's ratio and number of series terms

In order to verify the analytical approach, four studies are considered. The first one is an experimental study for plastic buckling of simply supported uniaxial compressed plates [67]. In the second study [45], the solution of '*plastic buckling paradox*' was sought in the mode of testing which had previously done in Ref. [67]. The authors applied the incremental theory of plate buckling and considered the boundary stresses introduced by the friction between the plate and the testing machine heads. For the pre-buckling stress analysis, an incremental finite element procedure was performed by ANSYS, so that the load was subdivided into a sequence of small increments. The material properties and dimensions of the plates were the same or similar to those in Ref. [67] as shown in Tables 1 and 2 respectively. The plate was divided into 80 rectangular elements and the boundary conditions were zero force on the two longitudinal edges, zero displacement on the lower edge in both directions. On the upper edge, uniform and zero displacements are applied in the longitudinal and transverse directions respectively. In the buckling analysis, the finite element procedure for plastic plate buckling described in Ref. [16], was generalized to the case of nonuniform pre-buckling stress state. In the third and fourth studies [16, 23], the finite element and funicular polygon methods are employed for plastic buckling of simply supported and fully clamped plates under uniaxial, biaxial or shear loads. The suggested algorithm (Fig. 2) can be changed for the uniaxial and biaxial loadings in which $N_{xy} = 0$. In these cases, new load ratios are defined as $\bar{\psi}_y = \frac{N_y}{N_x}$ and $\bar{\psi}_{xy} = \frac{N_{xy}}{N_x}$. The arrays of stiffness matrix (Eqs. 4) and the characteristic equation (Eq. 40) should be rewritten by the new load ratios. As a result, k_x will be obtained instead of k_s and then $\sigma_{x,cr} = \frac{k_x \pi^2 E}{12(1-\nu_e^2)} \left(\frac{t}{b}\right)^2$. Table 1 shows the boundary and load conditions and Ramberg-Osgood parameters in the experimental and numerical studies. In this section, the dimensions of parameters are represented by Imperial units to match the results found from the literatures.

Table 1 Boundary and loading conditions and mechanical properties in the considered studies (1 ksi = 6.895 MPa)

No.	Method	B.C.	L.C.	Material	$E \times 10^4$ (ksi)	$\sigma_{.7E}$ (ksi)	q	ν_e
1	Experimental	SSSS	Uniaxial	Al 14S – T6	1.07	63.2	19	0.33
	[67]							
2	FEM (ANSYS)	SSSS	Uniaxial	Al 14S – T6	1.07	63.2	19	0.33
	[45]							
3	Funicular polygon	CCCC	Shear	Al 14S – T6	1.07	63.2	19	0.33
	[23]							
4	FEM [16]	SSSS	Uniaxial	Al 24S - T	1	100	10	0.33
			Biaxial					
			Shear					
		CCCC	Uniaxial					

In Tables 2 and 3, the results of analytical approach ($h = 20$) are compared with those of experimental study [67], numerical analysis (ANSYS) [45] and funicular polygon method [23]. These comparisons show excellent agreement for both uniaxial loaded simply supported and shear loaded fully clamped plates. The maximum differences are less than 4%, 2.6% and 2% for the experimental, FE (ANSYS) and funicular polygon methods respectively.

Table 2 Comparison of critical uniaxial stresses for SSSS plates

Specimen		1a	6a	8a	9a	10a
[67]						
b (in.)		6.69	4.68	3.94	3.44	3.19
ϕ		4	4	4	4.5	4.5
λ		42.5	30.1	25.6	22.5	20.8
$\sigma_{x,cr}$ (psi)	[67]	21200	42800	53300	57800	61400
	[45]	21900	43200	54600	58600	61400
	Present	21871	43532	55343	60090	62030

Table 3 Comparison of critical shear stresses for CCCC square plates ($k_s^e = 14.6$)

λ	56.3	59.3	62	64.5	66.9	68.9	70.7	
τ_{cr}	[23]	34000	33000	32000	31000	30000	29000	28000
(psi)	Present	33463	32803	31421	30433	29701	29042	28135

k_s	Present	10.74	11.68	12.23	12.82	13.46	13.96	14.24
-------	---------	-------	-------	-------	-------	-------	-------	-------

In the fourth study [16], a finite element technique was used in conjunction with the Stowell's theory [2]. Thus, the incompressible material was considered (the Poisson's ratio was 0.5) during inelastic buckling. Here, the analytical approach is applied for two states: initially, the incompressible material is used ($\nu = 0.5$) to compare the analytical and numerical methods; and then, it is repeated using variable Poisson's ratio (Eq. 1) to compare the results of two situations. In Tables 4 and 5, the results are shown for the simply supported plates with aspect ratios 1 and 1.5 respectively which are under uniaxial and biaxial loads. Table 6 shows the results for the fully clamped and simply supported square plates under uniaxial and pure shear loads respectively. In Tables 4 and 5, there is no difference between the analytical and numerical methods when the incompressible material is supposed, likewise in Table 6, negligible difference (less than 0.5%) is seen.

In the last row of each section of Tables 4-6, results of the second state are compares. These comparisons show that due to variation of Poisson's ratio, in both uniaxial and shear loadings the inelastic buckling loads decrease. As expected, increasing λ makes more slender plate and less plasticity occurs prior to buckling. In Figures 3-5, the differences are obviously shown for the different aspect ratios, thickness ratios, boundary and loading conditions. As seen in these Figures, increasing the thickness ratio in all cases, the difference increases up to 18.8%. This upper bound only depends on the elastic Poisson's ratio and can be analytically expressed as $\frac{1-4\nu_0^2}{3}$. In addition, increasing the plate aspect ratio, slope of difference curve increases and reaches to a constant value for $\phi \geq 1$, $\phi \geq 4$ and $\phi \geq 5$ as seen in Figures 3-5 respectively.

Table 4 Comparison of critical stresses for SSSS square plates ($a = b = 20$ in.)

1		Uniaxial, ($\sigma_x \neq 0, \sigma_y = \tau = 0$) ($k_x^e = 4$)							
		t (in.)	2.39053	1.76752	1.36678	1.12019	0.96449	0.858	0.77867
		λ	8.3664	11.3152	14.6329	17.8541	20.7363	23.31	25.6848
$\sigma_{x,cr}$ (psi)	[16]		125000	115000	105000	95000	85000	75000	65000
	Present	(a) $\nu = 0.5$	125000	115000	105000	95000	85000	75000	65000
		(b) ν (Eq. 1)	124498	114060	103186	91521	79020	66556	55719
		$\frac{(a) - (b)}{(b)} \times 100$	0.4	0.82	1.8	3.8	7.6	12.7	16.7

k_x	Present	ν (Eq. 1)	0.944	1.58	2.39	3.16	3.68	3.92	3.98
2	Biaxial ($\sigma_y = \sigma_x, \tau = 0$) ($k_x^e = 2$)								
	t (in.)		5.26002	3.78569	2.77755	2.08258	1.60231	1.2998	1.125
	λ		3.8023	5.2831	7.2006	9.6035	12.4820	15.3870	17.7778
$\sigma_{x,cr}$ (psi)	[16]		125000	115000	105000	95000	85000	75000	65000
	Present	(a) $\nu = 0.5$	125000	115000	105000	95000	85000	75000	65000
		(b) ν (Eq. 1)	125253	115390	105457	95108	83810	70873	57507
		$\frac{(a) - (b)}{(b)} \times 100$		0.2	0.35	0.44	0.11	1.4	5.8
	k_x	Present	ν (Eq. 1)	0.196	0.349	0.592	0.95	1.41	1.82
3	Biaxial ($\sigma_y = 0.5\sigma_x, \tau = 0$) ($k_x^e = 2.667$)								
	t (in.)		2.42382	1.93707	1.58816	1.33364	1.15727	1.03884	0.94979
	λ		8.25144	10.3249	12.5932	14.9966	17.2821	19.2522	21.0573
$\sigma_{x,cr}$ (psi)	[16]		125000	115000	105000	95000	85000	75000	65000
	Present	(a) $\nu = 0.5$	125000	115000	105000	95000	85000	75000	65000
		(b) ν (Eq. 1)	125055	114703	103669	91570	78284	65671	55374
		$\frac{(a) - (b)}{(b)} \times 100$		0.04	0.26	1.3	3.8	8.6	14.2
	k_x	Present	ν (Eq. 1)	0.923	1.325	1.78	2.23	2.53	2.64

Table 5 Comparison of critical stresses for SSSS plates with $a = 30$ in. and $b = 20$ in.

1	Uniaxial ($\sigma_x \neq 0, \sigma_y = \tau = 0$) ($k_x^e = 4.694$)								
	t (in.)		2.45321	1.80884	1.39064	1.1271	0.95429	0.83518	0.75088
	λ		8.15258	11.0568	14.3819	17.7447	20.958	23.9469	26.6354
$\sigma_{x,cr}$ (psi)	[16]		125000	115000	105000	95000	85000	75000	65000
	Present	(a) $\nu = 0.5$	125000	115000	105000	95000	85000	75000	65000
		(b) ν (Eq. 1)	124520	114104	103296	91864	79835	67403	56059
		$\frac{(a) - (b)}{(b)} \times 100$		0.39	0.79	1.7	3.4	6.5	11.3
	k_x	Present	ν (Eq. 1)	0.897	1.511	2.315	3.134	3.799	4.188
2	Biaxial ($\sigma_y = \sigma_x, \tau = 0$) ($k_x^e = 2.778$)								
	t (in.)		4.46327	3.21226	2.35683	1.76713	1.3596	1.10292	0.9546
	λ		4.481	6.2261	8.486	11.3178	14.7102	18.1337	20.9512
	[16]		125000	115000	105000	95000	85000	75000	65000

$\sigma_{x,cr}$ (psi)	Present	(a)	$\nu = 0.5$	125000	115000	105000	95000	85000	75000	65000
		(b)	ν (Eq. 1)	125253	115390	105457	95108	83810	70873	57507
		$\frac{(a) - (b)}{(b)} \times 100$		0.2	0.34	0.44	0.11	1.4	5.8	13
k_x	Present	ν	(Eq. 1)	0.272	0.485	0.823	1.320	1.965	2.525	2.735
3	Biaxial ($\sigma_y = 0.5\sigma_x, \tau = 0$) ($k_x^e = 3.388$)									
		t (in.)		2.35015	1.84729	1.48109	1.21632	1.03918	0.92558	0.8437
		λ		8.5101	10.8267	13.5036	16.443	19.2459	21.6081	23.7051
$\sigma_{x,cr}$ (psi)	[16]			125000	115000	105000	95000	85000	75000	65000
Present	(a)	$\nu = 0.5$		125000	115000	105000	95000	85000	75000	65000
	(b)	ν (Eq. 1)		125100	114768	103845	91994	78873	66006	55471
		$\frac{(a) - (b)}{(b)} \times 100$		0.08	0.2	1.1	3.3	7.8	13.6	17.2
k_x	Present	ν	(Eq. 1)	0.982	1.458	2.052	2.695	3.165	3.339	3.377

Table 6 Comparison of critical stresses for square plates ($a = b = 20$ in.) with different boundary and loading conditions

1	CCCC - Uniaxial ($\sigma_x \neq 0, \sigma_y = \tau = 0$) ($k_x^e = 10.078$)						
	t (in.)			0.8	0.7	0.6	0.5
	λ			25	28.571	33.333	40
$\sigma_{x,cr}$ (psi)	[16]			97549	91234	81712	66414
	Present	(a)	$\nu = 0.5$	97130	91033	81714	66420
		(b)	ν (Eq. 1)	94216	86932	75525	57528
	$\frac{(a)-(b)}{(b)} \times 100$			3.1	4.7	8.2	15.5
k_x	Present	ν (Eq. 1)		6.38	7.689	9.092	9.973
2	SSSS - Shear ($\sigma_x = \sigma_y = 0, \tau \neq 0$) ($k_s^e = 9.34$)						
	t (in.)			0.7	0.6	0.5	0.4
	λ			28.571	33.333	40	50
τ_{cr} (psi)	[16]			60792	56604	50313	39414
	Present	(a)	$\nu = 0.5$	60760	56565	50251	39335
		(b)	ν (Eq. 1)	57132	52690	45578	33991
	$\frac{(a) - (b)}{(b)} \times 100$			6.4	7.4	10.3	15.7
k_s	Present	ν (Eq. 1)		5.053	6.343	7.901	9.207

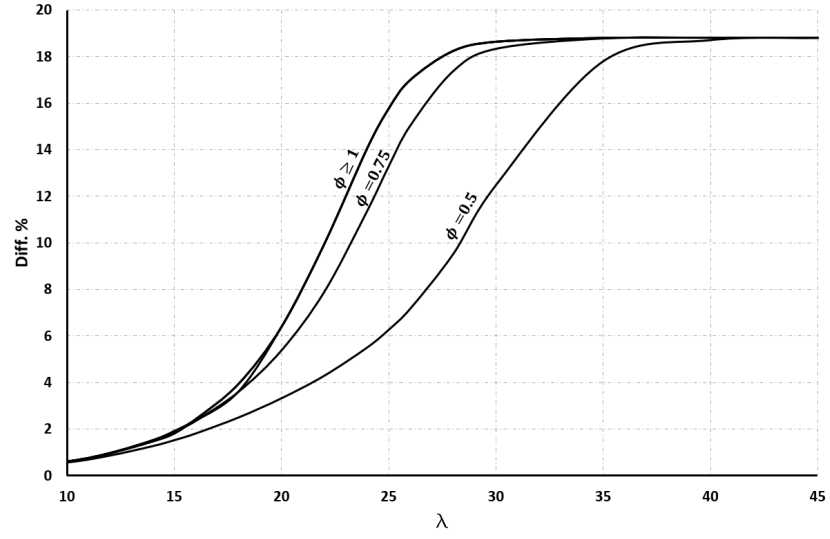


Fig. 3 Difference of $\sigma_{x,cr}(\nu = 0.5)$ and $\sigma_{x,cr}(\nu < 0.5)$ for a SSSS square plate under uniaxial load

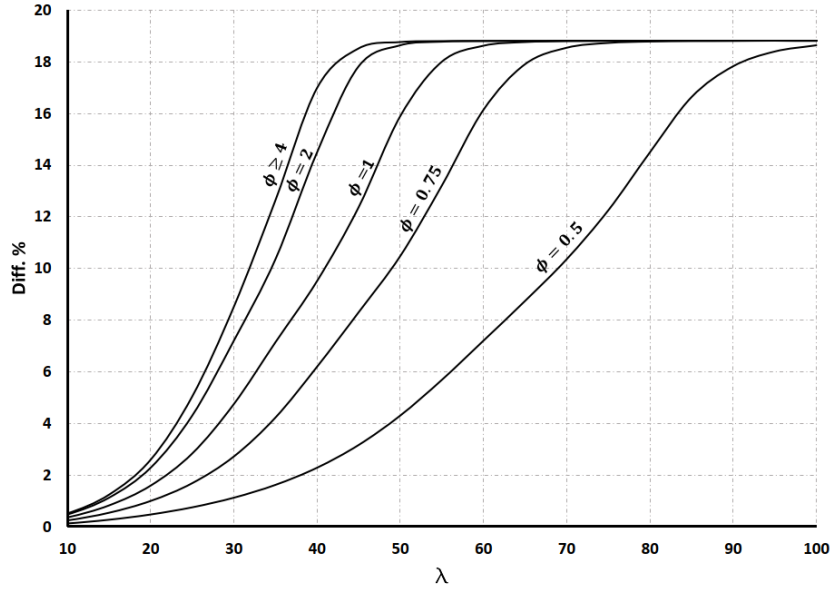


Fig. 4 Difference of $\tau_{cr}(\nu = 0.5)$ and $\tau_{cr}(\nu < 0.5)$ for a SSSS square plate under pure shear load

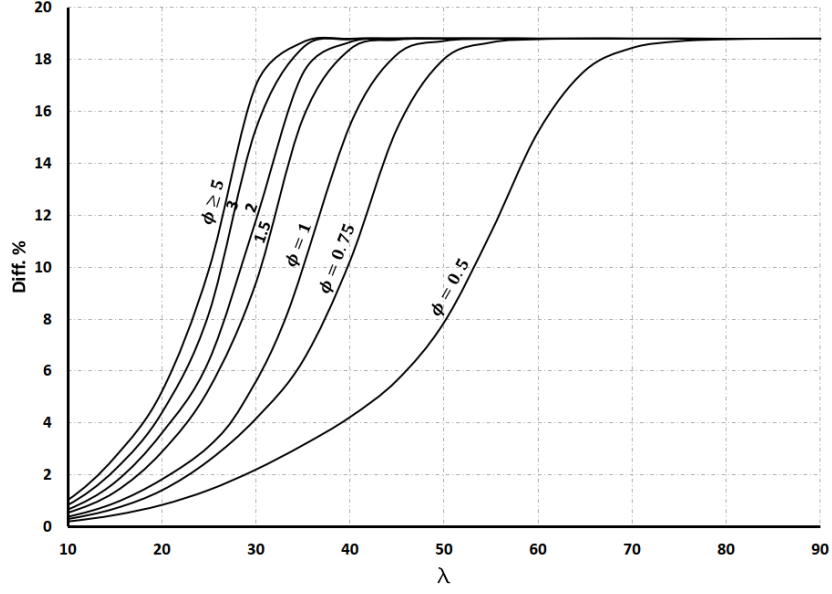


Fig. 5 Difference of $\sigma_{x,cr}(\nu = 0.5)$ and $\sigma_{x,cr}(\nu < 0.5)$ for a CCCC square plate under uniaxial stress

The number of series terms (h) directly effects on the accuracy of GITT. Table 7 shows a sensitivity analysis of inelastic buckling coefficient (k_s) with $\nu_e = 0.33$, $\frac{E}{\sigma_{0.7E}} = 100$ and $q = 10$. Considering this Table, it can be concluded that for small thickness ratios, k_s converges with 10 to 15 terms very well for all aspect ratios, boundary conditions and loading combinations. For larger thickness ratios, 20 terms are usually necessary for the convergence, although in TTS loading more terms may be used for more accuracy. However, 20 terms are used for the considered cases in this study.

Table 7 Convergence of k_s with different geometrical, boundary and loading conditions

ϕ	λ	h	SSSS								CCCC							
			ψ_x	ψ_y	ψ_x	ψ_y	ψ_x	ψ_y	ψ_x	ψ_y	ψ_x	ψ_y	ψ_x	ψ_y	ψ_x	ψ_y	ψ_x	ψ_y
			-1	-0.5	-1	0.5	1	-0.5	1	0.5	-1	-0.5	-1	0.5	1	-0.5	1	0.5
1	10	5	0.9899		0.7417		0.6788		0.6715		1.0692		0.7768		0.7159		0.7335	
		10	0.9855		0.7415		0.6788		0.6717		1.0654		0.7762		0.7157		0.7334	
		15	0.9851		0.7414		0.6788		0.6717		1.0650		0.7761		0.7157		0.7334	
		20	0.9851		0.7414		0.6788		0.6717		1.0649		0.7761		0.7157		0.7334	
		25	0.9850		0.7414		0.6788		0.6717		1.0649		0.7761		0.7157		0.7334	
		30	0.9850		0.7414		0.6788		0.6717		1.0649		0.7761		0.7157		0.7334	

100	5	55.087	12.0062	5.3478	2.4806	63.0118	18.1148	9.4169	5.7614
		54.552	11.9748	5.3423	2.4798	62.6175	17.9889	9.3967	5.7577
		54.512	11.9732	5.342	2.4798	62.5731	17.9835	9.3958	5.7575
		20	54.505	11.9730	5.342	2.4798	62.5625	17.9820	9.3956
		25	54.503	11.9729	5.342	2.4798	62.5586	17.9817	9.3955
		30	54.502	11.9729	5.342	2.4798	62.5574	17.9816	9.3955
	10	5	1.0799	0.6218	0.6629	0.6553	0.8936	0.7398	0.6727
		10	0.9270	0.6217	0.6552	0.6554	0.8894	0.7390	0.6549
		15	0.9266	0.6217	0.6551	0.6554	0.8894	0.7390	0.6548
		20	0.9265	0.6217	0.6551	0.6554	0.8893	0.7389	0.6548
		25	0.9265	0.6217	0.6551	0.6554	0.8893	0.7389	0.6548
		30	0.9265	0.6217	0.6551	0.6554	0.8893	0.7389	0.6548
4	100	5	64.622	2.4320	4.5781	1.8840	21.6047	11.5113	4.6996
		10	44.575	2.4293	4.0996	1.8807	20.2025	11.4142	4.0029
		15	44.493	2.4290	4.0958	1.8804	20.1751	11.4095	4.0006
		20	44.482	2.4290	4.0951	1.8803	20.1699	11.4086	4.0002
		25	44.479	2.4290	4.095	1.8803	20.1683	11.4083	4.0001
		30	44.477	2.4290	4.095	1.8803	20.1677	11.4082	4.0001

3.2 Estimation of inelastic buckling coefficient

In the proposed geometrical solution, the curves of $k_s = f(\xi, \phi, \psi_x, \psi_y, q, v_e)$ and $k_s = g(\xi, \psi_x, \psi_y, q, v_e, \lambda, \frac{E}{\sigma_{.7E}})$ are intersected in the $k_s - \xi$ plane to find k_s as well as the corresponding ξ . Figures 6 and 7 show some interaction curves in which f and g are plotted with solid and dashed curves respectively. In each Figure, $\frac{E}{\sigma_{.7E}}$, ψ_x , ψ_y , q and v_e are constants and ϕ and λ are variables to provide the interaction curves. In addition, the intersections of $\phi = 1$ curves and some λ curves are highlighted which are corresponded to the shown results in Table 3 and the second section of Table 6 respectively. The comparisons show the adequate accuracy of geometrical solution.

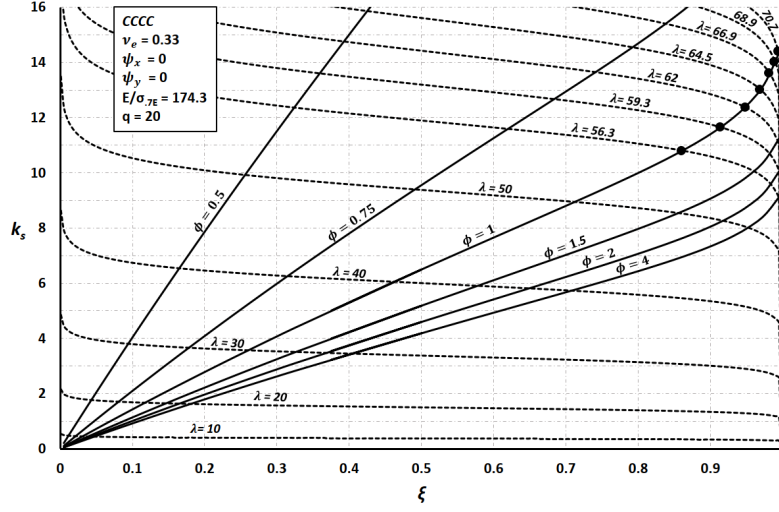


Fig. 6 Interaction curves of $k_s - \xi$ for fully clamped plates with $\psi_x = 0$ and $\psi_y = 0$

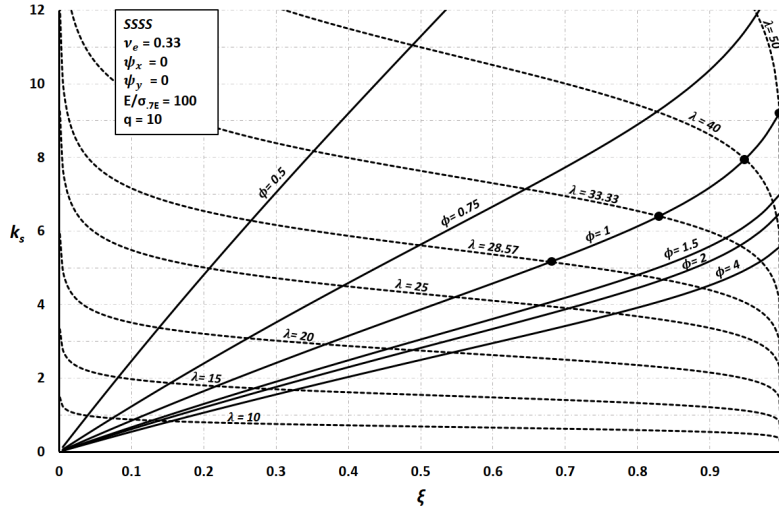


Fig. 7 Interaction curves of $k_s - \xi$ for simply supported plates with $\psi_x = 0$ and $\psi_y = 0$

In addition to the geometrical solution, a semi analytical approach may be supposed to simplify the calculation of inelastic buckling coefficient. The depicted Figures in Appendix A show that the variation of f with constant values of ν_e , ψ_x , ψ_y , ϕ and q may be estimated by linear or bilinear curves in the $k_s - \xi$ plane. Eq. (49) shows the general form of bilinear (or linear, if $C = 0$ and $S_1 = S_2$) description of k_s . If the correlation coefficient of the linear approximation, $R < 0.999$, then the bilinear curve is considered to estimate.

$$k_s = \begin{cases} S_1 \xi & ; \quad \xi \leq \bar{\xi} \\ S_2 \xi + C & ; \quad \xi > \bar{\xi} \end{cases} \quad (49)$$

where $\bar{\xi} = \frac{c}{s_1 - s_2}$. The depicted Figures in Appendix B show that S_1 , S_2 and C with a constant value of ν_e , ψ_x , ψ_y , ϕ may be estimated by linear curves in $S_1 - \ln q$, $S_2 - \ln q$ and $C - \ln q$ planes respectively. Thus,

$$\begin{bmatrix} S_1 \\ S_2 \\ C \end{bmatrix} = \begin{bmatrix} s_{11} & s_{12} \\ s_{21} & s_{22} \\ c_1 & c_2 \end{bmatrix} \begin{bmatrix} \ln q \\ 1 \end{bmatrix} \quad (50)$$

where s_{11} , s_{12} , s_{21} , s_{22} , c_1 and c_2 are numerically presented in Tables 8 and 9 for SSSS and CCCC plates respectively. The method of linear least squares (LLS) is applied in two stages on the results with $\phi = 1, 1.5, 2 \text{ \& } 4$, $\psi_x, \psi_y = -1, -0.5, 0, 0.5 \text{ \& } 1$, $q = 2, 3, 5, 10, 15 \text{ \& } 20$ and $\nu_e = 0.33$ to find S_1 , S_2 and C as well as s_{ij} ($i, j = 1, 2$) and c_i ($i = 1, 2$). If $\psi_x = \psi_y = -1$, then no shear buckling occurs in the plate and this case is naturally eliminated. In Tables 8 and 9, \bar{q} is the smallest integer of q , so that $R < 0.999$. Therefore, if $q < \bar{q}$ (i.e. $R \geq 0.999$), then the linear approximation must be considered and vice versa.

Substituting Eq. (49) into Eq. (48), q^{th} order equations will be obtained (Eqs. 51) which can be solved by trial and error method and usual scientific calculators. It can be shown that each of them always has a positive root which is the acceptable k_s .

$$\begin{cases} k_s^q + A^{q-1}k_s - A^{q-1}S_1 = 0 & ; A \leq \bar{A} \\ k_s^q - Ck_s^{q-1} + A^{q-1}k_s - A^{q-1}(S_2 + C) = 0 & ; A > \bar{A} \end{cases} \quad (51)$$

where

$$A = \frac{12(1 - \nu_e^2)\lambda^2}{\pi^2\Omega} \cdot \frac{\sigma_{7E}}{E} \left(\frac{7}{3}\right)^{\frac{1}{q-1}} \quad (52)$$

and

$$\bar{A} = S_1 \left(\frac{\bar{\xi}^q}{1 - \bar{\xi}} \right)^{\frac{1}{q-1}} \quad (53)$$

The semi-analytical approach can be summarized by a step by step procedure as follows:

- 1- Select s_{ij} ($i, j = 1, 2$), c_i ($i = 1, 2$) and \bar{q} from Tables 8 and 9 according to the boundary conditions and ν_e , ψ_x , ψ_y and ϕ . In this study, the fundamental parameters (s_{ij} & c_i) are obtained for SSSS and CCCC plates with $\nu_e = 0.33$, $\phi = 1, 1.5, 2 \text{ \& } 4$ and $\psi_x, \psi_y = -1, -0.5, 0, 0.5 \text{ \& } 1$ except $\psi_x = \psi_y = -1$. It is evident that the fundamental parameters can be also found for the other states.
- 2- If $q < \bar{q}$, then
 - 2-1- using the first equation of Eqs. (50), S_1 is calculated.

2-2- using Eq. (52), A is calculated by the known parameters: $\frac{E}{\sigma_{.7E}}$, Ω , λ , ν_e and q .

2-3- using the first equation of Eqs. (51), k_s is calculated by trial and error method.

3- If $q \geq \bar{q}$, then

3-1- S_1, S_2 and C are calculated using Eqs. (50) and then $\bar{\xi} = \frac{C}{S_1 - S_2}$.

3-2- Using Eqs. (52) and (53), A and \bar{A} are calculated respectively by the known parameters: $\frac{E}{\sigma_{.7E}}$, Ω , λ , ν_e and q .

3-3- If $A \leq \bar{A}$, then the first equation of Eqs. (51) is solved and k_s is calculated by trial and error method.

3-4- If $A > \bar{A}$, then the second equation of Eqs. (51) is solved and k_s is calculated by trial and error method.

Note that if $q = 2$ or $q = 3$, Eqs. (51) have the explicit solutions.

Table 8 Fundamental parameters for SSSS plates with $\nu_e = 0.33$

ψ_y	ψ_x	\bar{q}	s_{11}	s_{12}	s_{21}	s_{22}	c_1	c_2	\bar{q}	s_{11}	s_{12}	s_{21}	s_{22}	c_1	c_2
$\phi = 1$									$\phi = 1.5$						
-1	-0.5	-	-1.294	117.37	-	-	-	-	-	-0.968	93.12	-	-	-	-
	0	16	-0.711	29.43	6.007	26.62	-6.350	2.510	20	-0.499	24.46	3.770	24.13	-4.047	0.126
	0.5	9	-0.490	12.38	4.052	10.12	-4.228	2.152	10	-0.396	11.11	3.337	9.097	-3.482	1.901
	1	6	-0.347	6.942	2.727	5.565	-2.841	1.337	10	-0.242	6.231	1.970	5.052	-2.052	1.114
-0.5	-1	-	-1.294	117.37	-	-	-	-	-	-0.892	77.41	-	-	-	-
	-0.5	16	-0.936	38.87	8.026	34.81	-8.473	3.648	17	-0.655	29.35	5.581	26.63	-5.907	2.394
	0	6	-0.840	17.70	6.873	14.05	-7.164	3.538	8	-0.592	13.81	4.917	11.02	-5.125	2.679
	0.5	4	-0.615	9.482	5.220	6.292	-5.377	3.121	5	-0.433	7.471	3.713	5.048	-3.823	2.346
	1	4	-0.368	5.508	3.068	3.614	-3.158	1.854	4	-0.291	4.606	2.438	3.035	-2.509	1.530
0	-1	16	-0.713	29.43	6.007	26.62	-6.350	2.510	13	-0.524	18.01	5.070	14.10	-5.285	3.709
	-0.5	6	-0.840	17.70	6.873	14.05	-7.164	3.538	6	-0.561	11.22	4.551	8.944	-4.745	2.224
	0	3	-0.754	9.552	6.531	5.836	-6.692	3.672	4	-0.502	7.292	4.244	4.731	-4.371	2.515
	0.5	3	-0.521	5.467	4.426	3.087	-4.534	2.392	3	-0.373	4.977	3.169	3.137	-3.247	1.811
	1	3	-0.327	3.531	2.724	2.012	-2.789	1.517	3	-0.334	3.582	2.764	2.003	-2.828	1.573
0.5	-1	9	-0.490	12.38	4.052	10.12	-4.228	2.152	6	-0.341	6.873	2.734	5.556	-2.852	1.287
	-0.5	4	-0.615	9.482	5.220	6.292	-5.377	3.121	4	-0.338	4.698	2.893	2.947	-2.974	1.718
	0	3	-0.521	5.467	4.426	3.087	-4.534	2.392	3	-0.305	3.376	2.589	1.975	-2.653	1.405
	0.5	3	-0.406	3.521	3.366	1.746	-3.445	1.800	3	-0.261	2.591	2.163	1.404	-2.214	1.190
	1	4	-0.305	2.536	2.477	1.153	-2.533	1.391	3	-0.201	2.085	1.634	1.145	-1.672	0.935
1	-1	6	-0.347	6.942	2.727	5.566	-2.841	1.337	5	-0.169	3.182	1.459	2.215	-1.505	0.937
	-0.5	4	-0.367	5.508	3.063	3.621	-3.154	1.848	4	-0.185	2.470	1.506	1.603	-1.551	0.854
	0	3	-0.327	3.531	2.724	2.011	-2.789	1.517	3	-0.193	1.984	1.596	1.081	-1.633	0.901
	0.5	3	-0.305	2.536	2.477	1.153	-2.533	1.391	3	-0.195	1.662	1.578	0.757	-1.613	0.907
	1	2	-0.265	1.946	2.092	0.886	-2.131	1.067	3	-0.178	1.429	1.405	0.594	-1.435	0.833
$\phi = 2$									$\phi = 4$						
-1	-0.5	-	-0.852	85.27	-	-	-	-	-	-0.739	78.19	-	-	-	-
	0	-	-0.452	22.64	-	-	-	-	-	-0.374	20.59	-	-	-	-

	0.5	14	-0.311	10.27	2.424	9.325	-2.556	0.857	15	-0.274	9.520	2.158	8.618	-2.271	0.804
	1	10	-0.225	5.807	1.810	4.767	-1.888	0.984	12	-0.191	5.548	1.428	5.038	-1.503	0.471
-0.5	-1	-	-0.760	66.05	-	-	-	-	-	-0.623	56.31	-	-	-	-
	-0.5	19	-0.518	25.57	4.026	24.92	-4.314	0.427	20	-0.435	22.38	3.548	21.27	-3.781	0.859
	0	10	-0.500	12.68	4.207	10.14	-4.384	2.423	7	-0.401	11.21	3.430	9.018	-3.575	2.072
	0.5	5	-0.391	7.149	3.372	4.876	-3.472	2.190	7	-0.314	6.512	2.516	5.078	-2.616	1.380
	1	4	-0.290	4.588	2.415	3.040	-2.486	1.506	5	-0.225	4.225	1.903	2.911	-1.959	1.262
0	-1	13	-0.393	13.83	3.248	12.40	-3.425	1.305	15	-0.282	11.11	2.400	9.854	-2.532	1.145
	-0.5	7	-0.411	9.542	3.387	7.722	-3.532	1.751	8	-0.348	8.198	3.120	5.721	-3.232	2.374
	0	4	-0.479	6.782	4.097	3.997	-4.216	2.726	4	-0.354	5.810	3.020	3.807	-3.108	1.940
	0.5	3	-0.374	4.502	3.167	2.664	-3.243	1.817	3	-0.318	4.153	2.689	2.525	-2.753	1.594
	1	3	-0.261	3.178	2.188	1.891	-2.240	1.272	3	-0.235	3.033	1.956	1.840	-2.002	1.169
0.5	-1	6	-0.205	4.306	1.677	3.425	-1.746	0.852	17	-0.068	2.508	0.537	2.276	-0.574	0.227
	-0.5	4	-0.214	3.392	1.795	2.322	-1.850	1.044	13	-0.078	2.359	0.504	2.368	-0.538	-0.020
	0	3	-0.207	2.751	1.763	1.703	-1.806	1.030	11	-0.083	2.224	0.623	1.903	-0.654	0.306
	0.5	3	-0.184	2.308	1.526	1.396	-1.561	0.896	6	-0.150	2.167	1.617	-0.347	-1.636	2.419
	1	4	-0.162	2.010	1.205	1.176	-1.237	0.800	4	-0.187	1.982	1.568	0.438	-1.596	1.484
1	-1	5	-0.106	1.996	0.907	1.407	-0.934	0.566	7	-0.057	1.229	0.448	0.989	-0.468	0.232
	-0.5	4	-0.124	1.743	1.064	1.044	-1.091	0.681	5	-0.067	1.188	0.564	0.809	-0.581	0.365
	0	3	-0.136	1.533	1.124	0.871	-1.151	0.654	3	-0.076	1.152	0.613	0.726	-0.630	0.413
	0.5	3	-0.141	1.375	1.136	0.698	-1.161	0.672	4	-0.076	1.118	0.633	0.590	-0.648	0.512
	1	3	-0.129	1.248	1.026	0.574	-1.047	0.663	5	-0.081	1.103	0.516	0.681	-0.529	0.388

Table 9 Fundamental parameters for CCCC plates with $\nu_e = 0.33$

ψ_y	ψ_x	\bar{q}	s_{11}	s_{12}	s_{21}	s_{22}	c_1	c_2	\bar{q}	s_{11}	s_{12}	s_{21}	s_{22}	c_1	c_2
$\phi = 1$									$\phi = 1.5$						
-1	-0.5	-	-1.459	131.36	-	-	-	-	-	-1.147	104.15	-	-	-	-
	0	20	-0.803	37.53	6.014	36.95	-6.475	0.378	-	-0.649	30.23	-	-	-	-
	0.5	9	-0.716	18.43	5.967	14.88	-6.219	3.379	10	-0.542	15.04	4.573	12.14	-4.764	2.731
	1	5	-0.623	11.43	5.296	7.806	-5.453	3.456	7	-0.441	9.339	3.632	6.833	-3.768	2.405
-0.5	-1	-	-1.459	131.36	-	-	-	-	-	-0.944	89.15	-	-	-	-
	-0.5	-	-0.945	47.57	-	-	-	-	-	-0.697	36.15	-	-	-	-
	0	10	-0.855	23.74	7.260	19.22	-7.567	4.269	11	-0.623	18.58	4.885	16.62	-5.141	1.835
	0.5	5	-0.749	14.24	6.472	9.813	-6.664	4.253	6	-0.552	11.23	4.359	8.882	-4.540	2.277
	1	4	-0.630	9.625	5.239	6.225	-5.390	3.310	5	-0.451	7.572	3.780	5.013	-3.889	2.473
0	-1	20	-0.803	37.53	6.014	36.947	-6.475	0.378	18	-0.531	23.89	3.941	23.71	-4.248	0.082
	-0.5	10	-0.855	23.74	7.260	19.218	-7.567	4.269	11	-0.577	16.56	4.935	13.42	-5.145	2.958
	0	5	-0.825	15.11	7.113	10.292	-7.323	4.640	6	-0.588	11.86	4.657	9.308	-4.849	2.474
	0.5	4	-0.751	10.30	6.172	6.373	-6.349	3.849	4	-0.617	8.503	5.076	5.237	-5.220	3.196
	1	3	-0.620	7.453	5.095	4.300	-5.211	3.091	3	-0.508	6.188	4.179	3.602	-4.275	2.535
0.5	-1	9	-0.715	18.43	5.967	14.88	-6.219	3.379	8	-0.479	11.31	3.943	9.111	-4.109	2.103
	-0.5	5	-0.749	14.24	6.471	9.814	-6.663	4.252	5	-0.505	9.023	4.339	6.113	-4.468	2.809
	0	4	-0.751	10.30	6.172	6.373	-6.348	3.848	4	-0.528	7.316	4.340	4.492	-4.462	2.760
	0.5	3	-0.704	7.611	5.723	4.097	-5.850	3.460	3	-0.503	5.984	4.088	3.342	-4.177	2.576
	1	3	-0.636	5.901	5.028	2.739	-5.134	3.115	3	-0.543	5.066	4.185	1.753	-4.252	3.162
1	-1	5	-0.614	11.40	5.296	7.806	-5.453	3.456	5	-0.391	6.702	3.348	4.520	-3.448	2.115
	-0.5	4	-0.630	9.625	5.239	6.225	-5.390	3.310	4	-0.427	5.725	3.516	3.529	-3.617	2.156
	0	3	-0.620	7.453	5.095	4.300	-5.211	3.091	3	-0.450	4.900	3.684	2.661	-3.767	2.207
	0.5	3	-0.636	5.901	5.028	2.739	-5.134	3.115	3	-0.468	4.271	3.696	1.932	-3.773	2.304
	1	3	-0.624	4.810	4.785	1.670	-4.878	3.085	3	-0.451	3.767	3.433	1.437	-3.499	2.274
$\phi = 2$									$\phi = 4$						

-1	-0.5	-	-1.044	95.66	-	-	-	-	-	-	-0.948	88.41	-	-	-	-
	0	-	-0.582	27.75	-	-	-	-	-	-	-	-0.517	25.45	-	-	-
	0.5	13	-0.449	13.75	3.506	12.24	-3.687	1.393			14	-0.392	12.57	3.089	11.12	-3.244
	1	8	-0.366	8.494	2.943	6.752	-3.064	1.666			9	-0.318	7.784	2.578	6.186	-2.683
-0.5	-1	-	-0.798	77.12	-	-	-	-	-	-	-	-0.664	67.51	-	-	-
	-0.5	-	-0.587	32.36	-	-	-	-	-	-	-	-0.519	28.95	-	-	-
	0	12	-0.553	17.00	4.366	15.14	-4.594	1.728			14	-0.473	15.40	3.797	13.57	-3.987
	0.5	7	-0.494	10.34	3.920	8.160	-4.082	2.107			8	-0.420	9.447	3.374	7.430	-3.511
0	1	5	-0.405	6.999	3.404	4.659	-3.501	2.257			6	-0.346	6.443	2.680	4.894	-2.786
	-1	-	-0.429	20.50	-	-	-	-	-	-	-	-0.372	17.76	-	-	-
	-0.5	10	-0.548	15.05	4.675	12.10	-4.872	2.784			11	-0.450	13.24	3.630	11.52	-3.806
	0	6	-0.554	10.61	4.351	8.310	-4.531	2.243			6	-0.494	9.636	4.017	7.063	-4.170
0.5	0.5	4	-0.498	7.663	4.130	4.872	-4.246	2.708			4	-0.458	6.990	3.799	4.421	-3.906
	1	4	-0.472	5.804	3.968	2.547	-4.059	3.158			4	-0.394	5.249	3.193	2.922	-3.275
	-1	9	-0.364	9.141	3.035	7.347	-3.163	1.708			12	-0.279	8.055	2.680	5.335	-2.775
	-0.5	6	-0.410	7.879	3.238	6.113	-3.370	1.720			6	-0.395	7.272	3.112	5.394	-3.234
1	0	4	-0.457	6.776	3.762	4.113	-3.864	2.575			4	-0.473	6.230	3.860	3.704	-3.968
	0.5	3	-0.530	5.617	4.322	3.035	-4.419	2.554			3	-0.473	5.126	3.851	2.770	-3.937
	1	3	-0.457	4.533	3.626	2.262	-3.704	2.236			3	-0.431	4.203	3.445	1.857	-3.513
	-1	5	-0.307	5.266	2.629	3.521	-2.706	1.688			6	-0.214	4.336	1.697	3.396	-1.767
	-0.5	4	-0.351	4.787	2.893	2.924	-2.975	1.824			5	-0.257	4.225	2.122	2.680	-2.180
	0	3	-0.382	4.337	3.112	2.379	-3.180	1.919			3	-0.386	4.121	3.143	1.746	-3.205
	0.5	3	-0.416	3.978	3.217	1.821	-3.282	2.098			3	-0.453	3.789	3.562	1.538	-3.637
	1	3	-0.493	3.660	3.937	0.471	-3.999	3.099			3	-0.447	3.359	3.492	0.967	-3.557

The shown examples in Tables 3 and the second section of Table 6 are resolved using the suggested step by step procedure. Table 10 shows the obtained results for which the differences are less than 3%. In this Table, for CCCC and SSSS plates, $\xi > 0.8$ and $\xi > 0.6$ as seen in Figures 6 and 7 respectively. The semi-analytical method is also applied for SSSS and CCCC plates with four aspect ratios and load ratios (TTS, CTS, TCS and CCS) as shown in Tables 11 and 12 respectively. In these examples, the required Ramberg-Osgood parameters are $q = 10$ and $\frac{E}{\sigma_{.7E}} = 100$. For each aspect ratio in SSSS and CCCC plates, a maximum of four thickness ratios ($\lambda_i, i = 1, 2, 3, 4$) are selected provided that $\lambda_i = 5(j + 1)$; $j = 1, 2, 3, \dots$ and:

- (a) λ_1 is the last λ where $\xi_1 \leq 0.2$, otherwise is the first λ where $0.2 \leq \xi_1 \leq 0.3$.
- (b) λ_2 is the first λ where $0.3 \leq \xi_2 \leq 0.5$.
- (c) λ_3 is the first λ where $0.6 \leq \xi_3 \leq 0.8$.
- (d) λ_4 is the first λ where $0.9 \leq \xi_4 \leq 1$.

Tables 11 and 12 show that the difference between two methods are less than 12% for all examples. For each loading state, the maximum difference (M.D.) appears as follow:

- TTS loading: $10\% < \text{M.D.} < 12\%$ where $0.1 \leq \xi \leq 0.2$ for all plates.

- CTS loading: $5\% < \text{M.D.} < 7\%$ where $0.1 \leq \xi \leq 0.2$ for SSSS plates and $5\% < \text{M.D.} < 8\%$ where $0.1 \leq \xi \leq 0.2$ for CCCC plates.
- TCS loading: $7\% < \text{M.D.} < 11\%$ where $0.1 \leq \xi \leq 0.3$ for SSSS plates and $8\% < \text{M.D.} < 10\%$ where $0.1 \leq \xi \leq 0.2$ for CCCC plates.
- CCS loading: $2\% < \text{M.D.} < 10\%$ where $0.4 \leq \xi \leq 0.7$ for SSSS plates and $8\% < \text{M.D.} < 10\%$ where $0.2 \leq \xi \leq 0.3$ for CCCC plates.

In addition, the results show that increasing the thickness ratio in each aspect ratio, the differences are usually decreased. As a result, the semi-analytical method has more accuracy for $\lambda > 70$ in TTS loading and $\lambda > 20$ in CTS, TCS and CCS loadings. Of course, if $\frac{E}{\sigma_{.7E}}$, q , ψ_x and ψ_y are changed, the appeared differences may be slowly varied.

Table 10 Estimation of k_s for the shown examples in Table 3 and the second section of Table 6 ($\phi = 1$ and $\psi_x = \psi_y = 0$)

B.C.	$\frac{E}{\sigma_{.7E}}$	q	\bar{q}	S_1	S_2	C	$\bar{\xi}$	\bar{A}	λ	A	k_s		Diff. (%)	ξ
											Analytical Method	Eq. (51)		
CCCC	174.27	20	5	12.64	31.60	- 17.30	0.9122	13.04	56.3	11.90	10.74	10.83	0.8	0.8567
									59.3	13.20	11.68	11.64	0.3	0.9157
									62	14.43	12.23	12.46	1.9	0.9417
									64.5	15.61	12.82	13.15	2.6	0.9634
									66.9	16.80	13.46	13.68	1.6	0.9802
									68.9	17.82	13.96	13.99	0.2	0.9900
									70.4	18.60	14.24	14.13	0.8	0.9946
SSSS	100	10	3	7.816	20.87	- 11.74	0.8988	8.954	28.57	5.610	5.053	5.198	2.9	0.6651
									33.33	7.636	6.343	6.436	1.5	0.8234
									40	11.00	7.901	8.005	1.3	0.9457
									50	17.18	9.207	9.071	1.5	0.9968

Table 11 Estimation of k_s for SSSS plates with $q = 10$ and $\frac{E}{\sigma_{.7E}} = 100$

ψ_y	ψ_x	\bar{q}	ϕ	S_1	S_2	C	$\bar{\xi}$	\bar{A}	λ	A	k_s		Diff. (%)	ξ
											Analytical Method	Eq. (51)		
-1	-0.5	-	1	114.39	-	-	-	-	55	18.59	24.25	21.83	11.1	0.1909
									75	34.58	40.31	37.46	7.6	0.3274
									110	74.38	71.48	70.55	1.3	0.6168
									150	138.31	102.77	105.32	2.5	0.9207
		-	1.5	90.891	-	-	-	-	50	15.37	19.91	17.96	10.9	0.1976

									65	25.97	30.63	28.36	8	0.3120
									100	61.47	58.37	57.78	1	0.6357
									135	112.03	82.30	84.34	2.5	0.9279
									45	12.45	16.45	14.76	11.4	0.1772
									65	25.97	30.09	28.01	7.4	0.3362
									95	55.48	52.96	52.34	1.2	0.6282
									125	96.05	73.27	75.10	2.5	0.9015
									45	12.45	16.23	14.61	11.1	0.1911
									60	22.13	26.04	24.12	8	0.3154
									90	49.79	47.90	47.22	1.4	0.6173
									120	88.52	67.39	69.08	2.5	0.9031
									10	0.546	0.708	0.666	6.3	0.1430
									20	2.185	2.202	2.210	0.4	0.4742
									25	3.414	3.074	3.147	2.4	0.6752
									35	6.691	4.713	4.773	1.3	0.9543
									10	0.546	0.691	0.654	5.7	0.1660
									15	1.229	1.353	1.325	2.1	0.3367
									25	3.414	2.936	3	2.2	0.7621
									30	4.916	3.754	3.732	0.6	0.9226
									10	0.546	0.689	0.653	5.5	0.1666
									15	1.229	1.351	1.324	2	0.3378
									25	3.414	2.933	2.996	2.1	0.7642
									30	4.916	3.732	3.713	0.5	0.9260
									10	0.546	0.687	0.649	5.9	0.1750
									15	1.229	1.343	1.314	2.2	0.3544
									25	3.414	2.887	2.940	1.8	0.7932
									30	4.916	3.586	3.614	0.8	0.9410
									15	1.229	1.663	1.512	10	0.1343
									25	3.414	3.878	3.696	4.9	0.3285
									40	8.739	7.791	7.933	1.8	0.7050
									50	13.65	10.33	10.38	0.5	0.9221
									10	0.546	0.757	0.687	10.2	0.1128
									20	2.184	2.383	2.308	3.2	0.3791
									30	4.916	4.314	4.414	2.3	0.7250
									40	8.739	6.047	6.114	1.1	0.9614
									10	0.546	0.708	0.651	8.8	0.1699
									15	1.229	1.376	1.320	4.2	0.3443
									25	3.414	2.906	2.974	2.3	0.7757
									30	4.916	3.626	3.650	0.7	0.9358
									10	0.546	0.656	0.613	7	0.2608
									15	1.229	1.236	1.219	1.4	0.5184
									20	2.185	1.836	1.876	2.2	0.7978
									25	3.414	2.310	2.289	0.9	0.9734
									10	0.595	0.556	0.607	9.2	0.4547
									15	1.339	1.155	1.117	3.4	0.8363
									20	2.381	1.629	1.655	1.6	0.9635
									10	0.595	0.541	0.578	6.8	0.5668
									15	1.339	1.039	1.030	0.9	0.9142
									20	2.381	1.357	1.337	1.5	0.9945
									10	0.595	0.544	0.569	4.6	0.5987
									15	1.339	0.989	0.997	0.8	0.9346
									20	2.381	1.205	1.183	1.9	0.9981
									10	0.595	0.551	0.565	2.5	0.6161
									15	1.339	0.947	0.954	0.7	0.9547
									20	2.381	1.047	1.038	0.9	0.9994

Table 12 Estimation of k_s for CCCC plates with $q = 10$ and $\frac{E}{\sigma_{7E}} = 100$

ψ_y	ψ_x	\bar{q}	ϕ	S_1	S_2	C	$\bar{\xi}$	\bar{A}	λ	A	k_s		Diff. (%)	ξ
											Analytical Method	Eq. (51)		
-1	-0.5	-	1	128.00	-	-	-	-	55	18.60	24.62	22.13	11.3	0.1729
									80	39.34	45.63	42.52	7.3	0.3322
									115	81.30	78.69	77.51	1.5	0.6056
									155	147.69	112.74	115.43	2.4	0.9018
		-	1.5	101.51	-	-	-	-	50	15.37	20.21	18.20	11	0.1793
									70	30.12	35.17	32.71	7.5	0.3223
									105	67.77	64.59	63.90	1.1	0.6295
									140	120.49	90.58	92.73	2.4	0.9135
		-	2	93.26	-	-	-	-	50	15.37	19.93	18.01	10.7	0.1932
									65	25.97	30.70	28.46	7.9	0.3052
									100	61.47	58.82	58.13	1.2	0.6233
									135	112.03	83.67	85.63	2.3	0.9182
		-	4	86.23	-	-	-	-	45	12.45	16.47	14.82	11.1	0.1720
									65	25.97	30.21	28.15	7.3	0.3264
									95	55.48	53.49	52.75	1.4	0.6117
									130	103.89	77.47	79.27	2.3	0.9194
-0.5	1	4	1	8.174	18.30	-9.100	0.899	9.362	15	1.229	1.533	1.456	5.3	0.1782
									25	3.414	3.532	3.521	0.3	0.4308
									35	6.691	5.849	5.984	2.3	0.7320
									45	11.06	8.039	8.120	1	0.9417
		5	1.5	6.534	13.72	-6.482	0.902	7.542	10	0.546	0.743	0.692	7.4	0.1060
									20	2.185	2.378	2.332	2	0.3570
									30	4.916	4.407	4.500	2.1	0.6888
									40	8.739	6.369	6.425	0.9	0.9409
		5	2	6.066	12.50	-5.804	0.903	7.013	10	0.546	0.737	0.687	7.3	0.1132
									20	2.185	2.345	2.307	1.6	0.3802
									30	4.916	4.318	4.409	2.1	0.7268
									40	8.739	6.106	6.170	1	0.9582
		6	4	5.646	11.06	-4.911	0.906	6.585	10	0.546	0.730	0.681	7.2	0.1206
									20	2.185	2.313	2.281	1.4	0.4040
									30	4.916	4.226	4.314	2.1	0.7641
									35	6.691	5.187	5.168	0.4	0.9109
0.5	-1	9	1	16.78	28.62	-10.94	0.924	20.49	20	2.185	2.883	2.634	9.5	0.1569
									30	4.916	5.631	5.349	5.3	0.3187
									45	11.06	10.39	10.46	0.7	0.6232
									60	19.66	15.13	15.24	0.7	0.9082
		8	1.5	10.21	18.19	-7.358	0.922	12.37	15	1.229	1.639	1.495	9.6	0.1464
									25	3.414	3.797	3.644	4.2	0.3570
									35	6.691	6.281	6.335	0.9	0.6206
									50	13.655	9.799	9.888	0.9	0.9481
		9	2	8.303	14.34	-5.575	0.924	10.13	15	1.229	1.591	1.459	9	0.1757
									25	3.414	3.632	3.530	2.9	0.4252
									35	6.691	5.898	6.011	1.9	0.7240
									45	11.06	7.947	8.013	0.8	0.9479
		12	4	7.413	11.51	-3.794	0.927	9.108	15	1.229	1.564	1.439	8.7	0.1942
									20	2.185	2.503	2.375	5.4	0.3204
									30	4.916	4.610	4.642	0.7	0.6262
									40	8.739	6.704	6.751	0.7	0.9108
1	1	3	1	3.373	12.69	-8.147	0.875	3.661	10	0.595	0.629	0.692	10	0.2051
									15	1.339	1.269	1.393	9.8	0.4129
									20	2.381	2.097	2.215	5.6	0.6567
									30	5.357	3.832	3.880	1.3	0.9479
		3	1.5	2.729	9.342	-5.783	0.874	2.960	10	0.595	0.621	0.674	8.5	0.2469

								15	1.339	1.247	1.344	7.8	0.4925
								20	2.381	2.068	2.088	1	0.7652
								25	3.720	2.835	2.828	0.2	0.9218
								10	0.595	0.602	0.667	10.8	0.2642
3	2	2.525	9.536	-6.109	0.871	2.721	15	1.339	1.214	1.325	9.1	0.5246	
							20	2.381	2.061	2.033	1.4	0.8053	
							25	3.720	2.769	2.780	0.4	0.9322	
								10	0.595	0.597	0.660	10.6	0.2832
3	4	2.330	9.008	-5.838	0.874	2.527	15	1.339	1.204	1.304	8.3	0.5597	
							20	2.381	2.061	1.971	4.6	0.8458	
							25	3.720	2.663	2.697	1.3	0.9476	

4 Conclusion

An analytical approach is presented to obtain the inelastic buckling coefficient of simply supported and fully clamped rectangular plates subjected to combined biaxial (both compressive and tensile) and shear loads. The deformation theory of plasticity, variations to all mechanical properties of plate, the generalized integral transform technique (GITT) and eigenvalue solution are applied in the different sequences to obtain the inelastic buckling coefficient of plate. Ramberg-Osgood parameters are used to describe the nonlinear stress-strain behavior of material, although the solution can be generalized for the other nonlinear behaviors. Then applying the method of linear least squares (LLS) on the obtained results, a semi-analytical solution is also proposed. An approximate polynomial equation is obtained and solved by trial and error method to simplify the calculation of the inelastic buckling coefficient. The proposed semi-analytical solution is simple and applicable for the practical purposes. The calculated results show that good accuracy may be obtained for all loading cases, so that the maximum difference (less than 12%) is seen in tensile-tensile-shear loading state; nevertheless, increasing thickness ratio of plate, the accuracy increases.

Appendix A: Linear / Bilinear approximation of $k_s = f(\xi; \phi, \psi_x, \psi_y, q, \nu_e)$

Supposing the boundary conditions of plate and the specific values for $0 < \nu_e < 0.5$, $1 \leq \phi \leq 4$, $-1 \leq \psi_x \leq 1$, $-1 \leq \psi_y \leq 1$ and $2 \leq q \leq 20$, the suggested algorithm (Fig. 2) is applied and several examples may be solved to obtain the curves of $k_s - \xi$. Figs. A1-A12 show the obtained curves for some examples in which the curves of SSSS and CCCC plates are drawn in Figs. A1-A6 and Figs. A7-A12 respectively. In these Figures, $\nu_e = 0.33$, $\phi = 1, 1.5, 2, 4$, $\psi_x = -0.5, 1$, $\psi_y = -1, 1$ and $q = 3, 10, 20$. Initially, the method of linear least squares (LLS) is used and the correlation coefficient (R) of linear estimation is obtained for each curve as shown in Figs. A1-A12. If $R \geq 0.999$ the linear estimation is proposed; otherwise, the bilinear estimation (Eq. 49) is replaced to improve the approximation. In Figs.

A1-A12, the linear / bilinear approximations are only plotted for $\phi = 1$ (the dashed lines). The similar approximated curves can be evidently plotted for the other aspect ratios. Supposing constant values of q and ϕ and increasing ψ_x and ψ_y , the linear estimations are mostly converted to the bilinear estimations. If $R = 0.999$, the boundary of conversion is found for which the integer value of corresponding q is only considered (\bar{q} in Tables 8 and 9). For example, if $\phi = 4$ and $\psi_x = \psi_y = 1$, then $\bar{q} = 5$ for SSSS plates; thus, if $q = 3$ or $q = 10$, then $R = 0.9996$ (linear estimation, Fig. A2) or $R = 0.9964$ (bilinear estimation, Fig. A4).

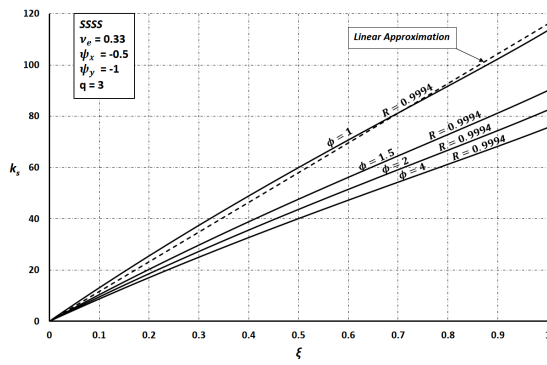


Fig. A1 Linear approximations of $k_s - \xi$ curves for all aspect ratios

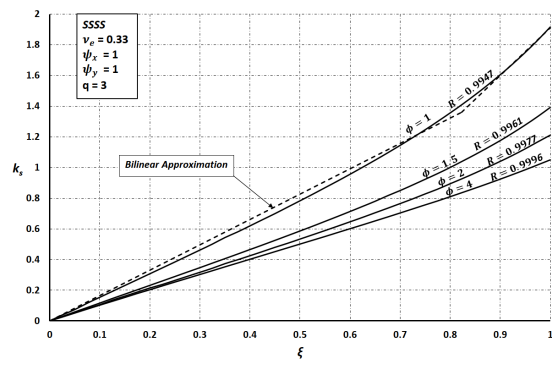


Fig. A2 Bilinear and linear approximations of $k_s - \xi$ curves for $\phi = 1, 1.5, 2$ and $\phi = 4$ respectively

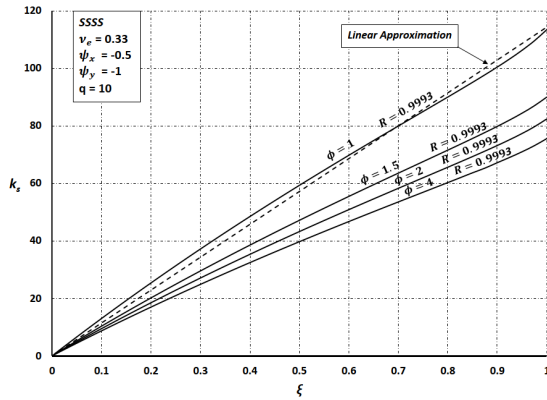


Fig. A3 Linear approximations of $k_s - \xi$ curves for all aspect ratios

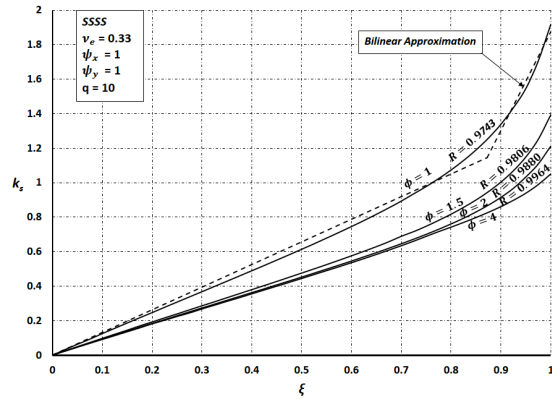


Fig. A4 Bilinear approximations of $k_s - \xi$ curves for all aspect ratios

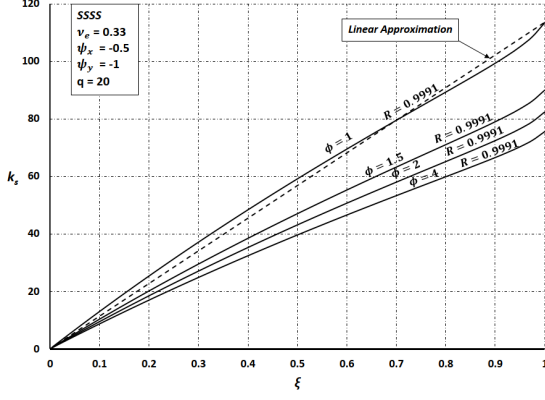


Fig. A5 Linear approximations of $k_s - \xi$ curves for all aspect ratios

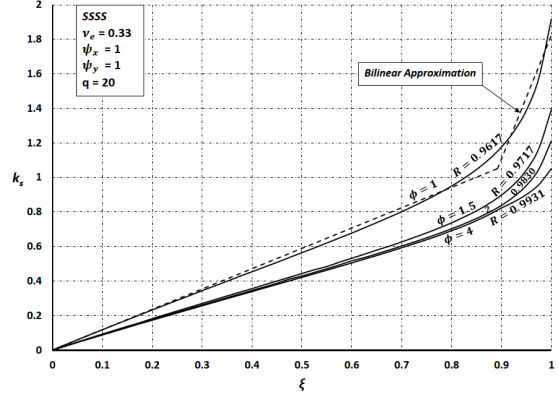


Fig. A6 Bilinear approximations of $k_s - \xi$ curves for all aspect ratios

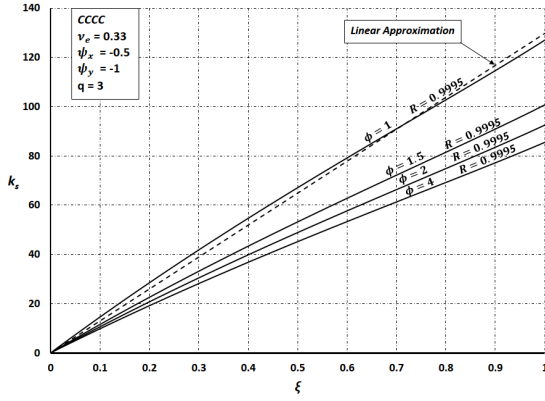


Fig. A7 Linear approximations of $k_s - \xi$ curves for all aspect ratios

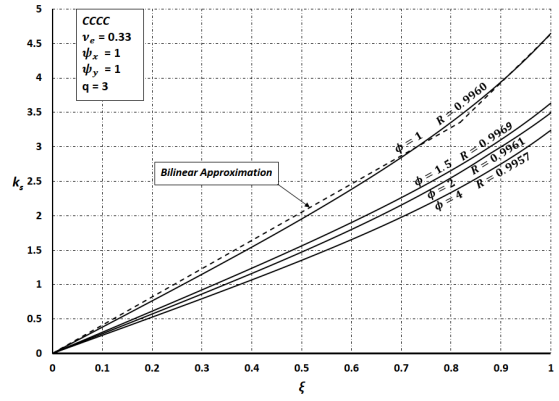


Fig. A8 Bilinear approximations of $k_s - \xi$ curves for all aspect ratios

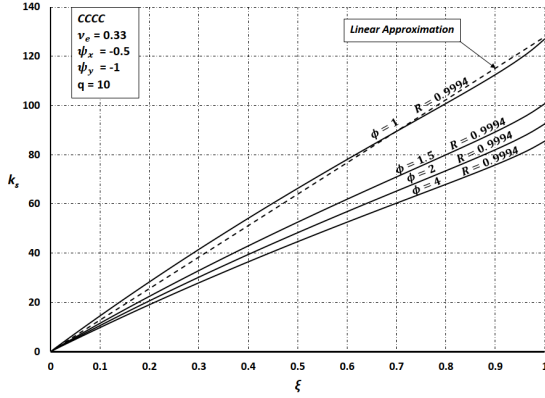


Fig. A9 Linear approximations of $k_s - \xi$ curves for all aspect ratios

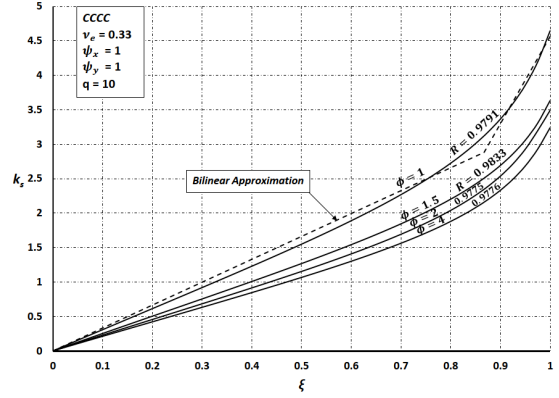


Fig. A10 Bilinear approximations of $k_s - \xi$ curves for all aspect ratios

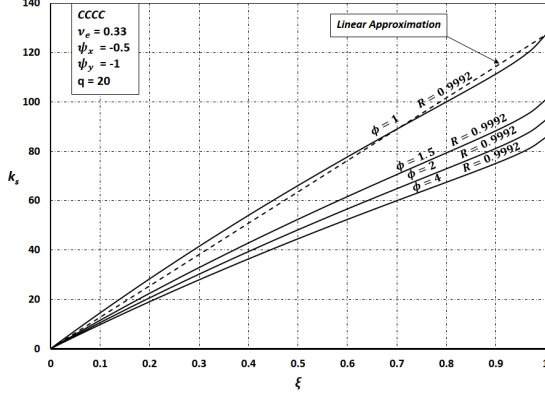


Fig. A11 Linear approximations of $k_s - \xi$ curves for all aspect ratios

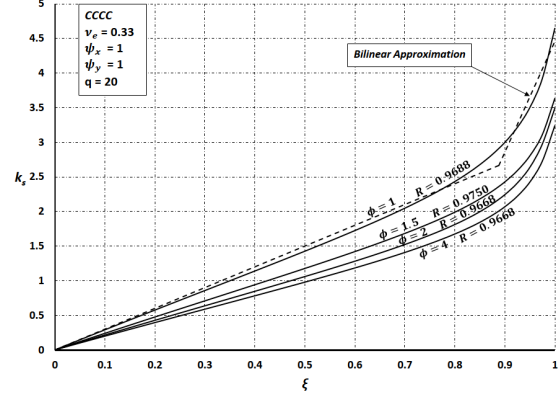


Fig. A12 Bilinear approximations of $k_s - \xi$ curves for all aspect ratios

Appendix B: Semi-logarithm estimation of S_1 , S_2 and C

In Appendix A and Eq. (49), a bilinear approximation is described with both slopes of lines (S_1 and S_2) and intercept of the second line (C) while a linear approximation is only described with slope of a line (S_1). Applying the method of linear least squares (LLS) on several examples, S_1 , S_2 and C can be linearly estimated versus $\ln q$. Figs. B1-B4 and B5-B8 show the estimations for SSSS and CCCC plates respectively. If linear approximation is applied on $k_s - \xi$ curves, then S_1 is only estimated as shown in Figs. B1 and B5 ($\psi_x = -0.5$, $\psi_y = -1$); if bilinear approximation is applied, then S_1 (Figs. B2 and B6), S_2 (B3 and B7) and C (B4 and B8) are estimated ($\psi_x = \psi_y = 1$). Eqs. (B1) show the semi-logarithm estimation,

$$\begin{cases} S_1 = s_{11} \ln q + s_{12} \\ S_2 = s_{21} \ln q + s_{22} \\ C = c_1 \ln q + c_2 \end{cases} \quad \text{B1}$$

where s_{11} , s_{21} and c_1 are the slopes and s_{12} , s_{22} and c_2 are the intercept of S_1 , S_2 and C respectively. For SSSS plates with $\phi = 1$, $\psi_x = -0.5$ and $\psi_y = -1$, Fig. B1 shows that $s_{11} = -1.294$ and $s_{12} = 117.37$. Similarly, the parameters of Eq. (B1) will be obtained for the different boundary and load conditions as shown in Table 8 and 9. The obtained correlation coefficients show that the semi-logarithm estimation is acceptable in this step.

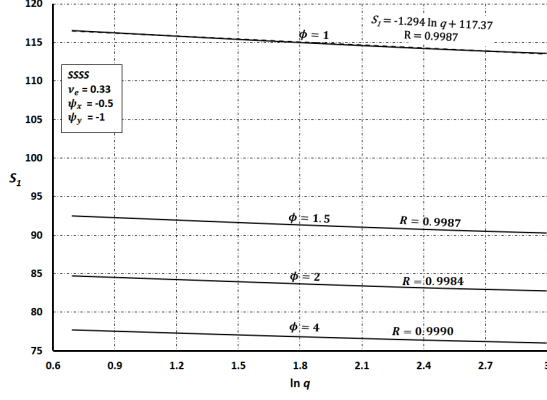


Fig. B1 Linear approximation of $S_1 - \ln q$ in Figs. A1, A3 and A5

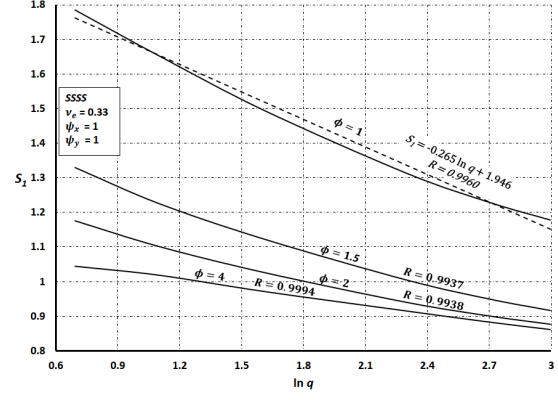


Fig. B2 Linear approximation of $S_1 - \ln q$ in Fig. A2, A4 and A6

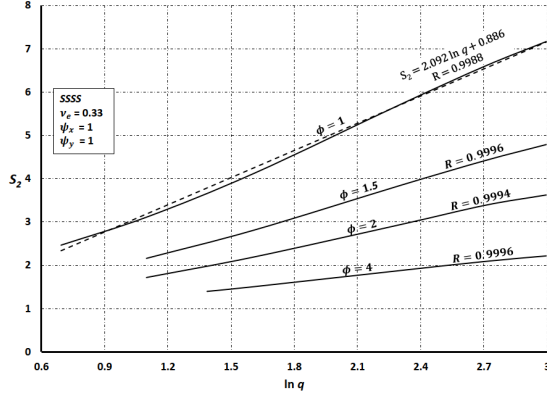


Fig. B3 Linear approximation of $S_2 - \ln q$ in Figs. A2, A4 and A6

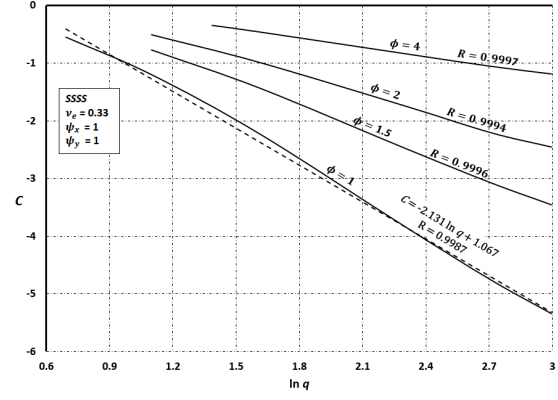


Fig. B4 Linear approximation of $C - \ln q$ in Figs. A2, A4 and A6

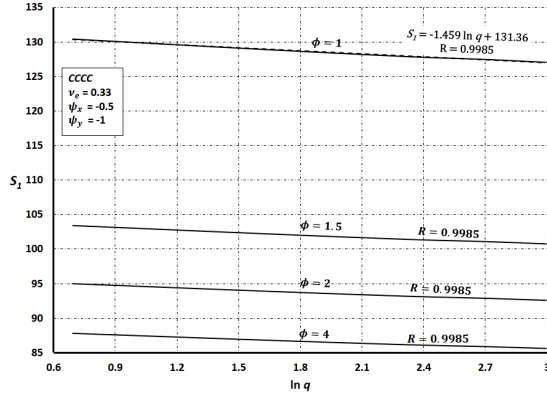


Fig. B5 Linear approximation of $S_1 - \ln q$ in Figs. A7, A9 and A11

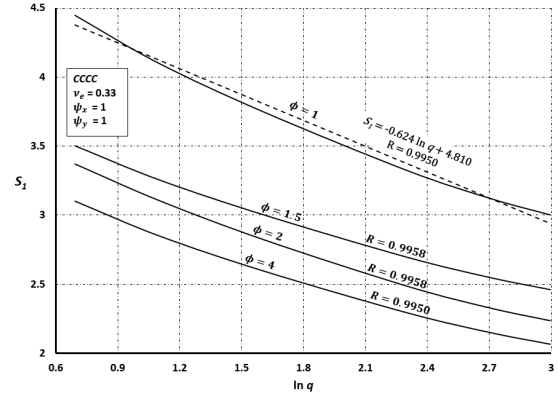


Fig. B6 Linear approximation of $S_1 - \ln q$ in Fig. A8, A10 and A12

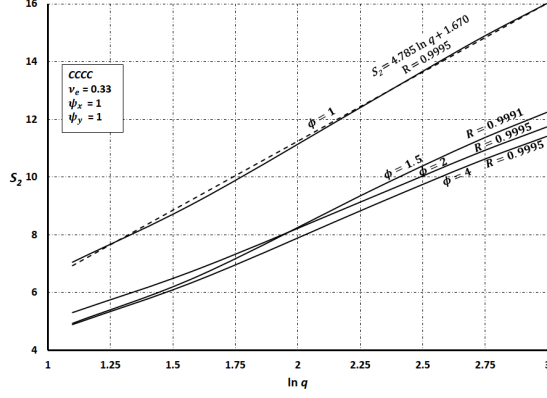


Fig. B7 Linear approximation of $S_2 - \ln q$ in Fig. A8, A10 and A12

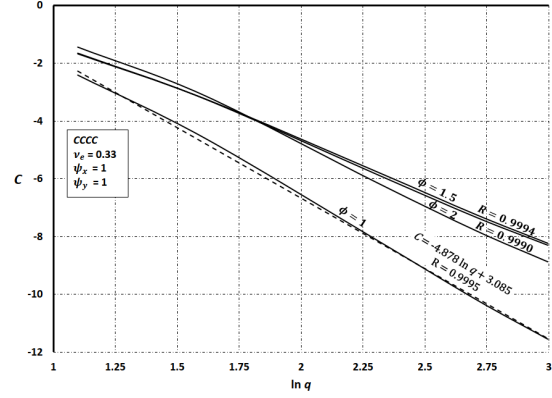


Fig. B8 Linear approximation of $C - \ln q$ in Fig. A8, A10 and A12

Notations

a	Length of plate
b	Width of plate
h	Number of series terms in the GITT
k_s, k_x	Inelastic buckling coefficients
k_s^e, k_x^e	Elastic buckling coefficients
m, n, r, s	Positive integers
q	Shape parameter to describe the curvature of stress-strain curve in the Ramberg-Osgood representation
\bar{q}	Integer of corresponding q in the boundary of linear and bilinear approximations ($R = 0.999$)
s_{ij}, c_i	Fundamental parameters to find S_1, S_2 and C ($i, j = 1, 2$)
t	Thickness of plate
z	Distance from the middle surface of plate
C	Intercept of the second line in bilinear approximation of $k_s - \xi$ curve
D_{ij}	Arrays of stiffness matrix ($i, j = 1, 2, 3$)
E	Young's modulus (or the slop of stress-stain curve at zero stress)
E_{sec}	Secant modulus
E_{tan}	Tangent modulus
M_{mn}^{rs}	Arrays of coefficient matrix ($m, n, r, s = 1, 2, \dots, h$)
N_x, N_y, N_{xy}	In-plane loads in the x -, y - and xy - directions per unit length
R	Correlation coefficient of linear approximation in linear least squares
S_1, S_2	Slope of the first and the second line for approximation of $k_s - \xi$ curve
$X_m(x), Y_n(y)$	Kernels of double integral transform in x - and y -direction ($m, n = 1, 2, \dots, h$)
α_m, β_n	Roots of transcendental beam frequency equations in x - and y - directions ($m, n = 1, 2, \dots, h$)
γ	Shear strain
$\delta w(x, y)$	Variation of out of plane displacements in z - direction
δw_{mn}	Variation of transformed out of plane displacements ($m, n = 1, 2, \dots, h$)

$\delta M_x, \delta M_y$	Variation of bending moments in the x - and y - directions per unit length
δM_{xy}	Variation of twisting moment per unit length
$\delta \gamma_0$	Variation of middle surface shear strain
$\delta \varepsilon_{0x}, \delta \varepsilon_{0y}$	Variation of middle surface strains in x - and y - directions
$\delta \kappa_x, \delta \kappa_y$	Variation of curvatures in x - and y - directions
$\delta \kappa_{xy}$	Variation of twist
$\delta \sigma_x, \delta \sigma_y$	Variation of stresses in x - and y - directions
$\delta \tau$	Variation of shear stress
$\varepsilon_x, \varepsilon_y$	Strain in x - and y - directions
ξ	Secant modulus to Young's modulus ratio
η	Tangent modulus to Secant modulus ratio
λ	Thickness ratio of plate
ν	Poisson's ratio
ν_e	Elastic Poisson's ratio
$\sigma_{.7E}$	Stress corresponding to intersection of the stress-strain curve and a secant of $0.7E$ in Ramberg-Osgood representation
σ_i	Stress intensity
σ_x, σ_y	Stresses in x - and y - directions
τ	Shear stress
$\sigma_{x,cr}, \tau_{cr}$	Critical stresses
ϕ	Aspect ratio of plate
$\psi_x, \psi_y, \bar{\psi}_y, \bar{\psi}_{xy}$	Load ratios

References

1. Ilyushin, A.A., *The elastic-plastic stability of plates*. 1947, NACA, Technical Memorandum, No. 1188.
2. Stowell, E.Z., *A unified theory of plastic buckling*. 1948, NACA, Technical Note, No. 1556.
3. Bijlaard, P.P., *Theory and tests on the plastic stability of plates and shells*. Journal of the Aeronautical Sciences, 1949. **16**(9): p. 529-541.DOI: <https://doi.org/10.2514/8.11851>.
4. Handelman, G., Prager, W., *Plastic buckling of a rectangular plate under edge thrusts*. 1948, NACA, Technical Note, No. 1530.
5. Budiansky, B., *A Reassessment of Deformation Theories of Plasticity*. Journal of Applied Mechanics, 1959. **26**(2).
6. Jones, R.M., *Deformation theory of plasticity*. 2009: Bull Ridge Corporation.
7. Hutchinson, J.W., *Plastic buckling*. Advances in applied mechanics, 1974. **14**: p. 67-144.DOI: [https://doi.org/10.1016/S0065-2156\(08\)70031-0](https://doi.org/10.1016/S0065-2156(08)70031-0).

8. Guarracino, F., *Remarks on the stability analysis of some thin-walled structures in the elastic-plastic range*. Thin-Walled Structures, 2019. **138**: p. 208-214.DOI: <https://doi.org/10.1016/j.tws.2019.01.044>.
9. Becque, J., *The application of plastic flow theory to inelastic column buckling*. International Journal of Mechanical Sciences, 2016. **111-112**: p. 116-124.DOI: <https://doi.org/10.1016/j.ijmecsci.2016.04.005>.
10. Hutchinson, J.W., Budiansky, B., *Analytical and Numerical Study of the Effects of Initial Imperfections on the Inelastic Buckling of a Cruciform Column*, in *Buckling of Structures*, B. Budiansky, Editor. 1976, Springer Berlin Heidelberg: Berlin, Heidelberg. p. 98-105.DOI: https://doi.org/10.1007/978-3-642-50992-6_10.
11. Onat, E.T., Drucker, D.C., *Inelastic Instability and Incremental Theories of Plasticity*. Journal of the Aeronautical Sciences, 1953. **20**(3): p. 181-186.DOI: <https://doi.org/10.2514/8.2585>.
12. Guarracino, F., Simonelli, M.G., *The torsional instability of a cruciform column in the plastic range: Analysis of an old conundrum*. Thin-Walled Structures, 2017. **113**: p. 273-286.DOI: <https://doi.org/10.1016/j.tws.2016.11.007>.
13. Shamass, R., Alfano, G., Guarracino, F., *A numerical investigation into the plastic buckling paradox for circular cylindrical shells under axial compression*. Engineering Structures, 2014. **75**: p. 429-447.DOI: <https://doi.org/10.1016/j.engstruct.2014.05.050>.
14. Shamass, R., Alfano, G., Guarracino, F., *An investigation into the plastic buckling paradox for circular cylindrical shells under non-proportional loading*. Thin-Walled Structures, 2015. **95**: p. 347-362.DOI: <https://doi.org/10.1016/j.tws.2015.07.020>.
15. Shamass, R., *Plastic Buckling Paradox: An Updated Review*. Frontiers in Built Environment, 2020. **6**.DOI: <https://doi.org/10.3389/fbuil.2020.00035>.
16. Pifko, A., Isakson, G., *A finite-element method for the plastic buckling analysis of plates*. AIAA Journal, 1969. **7**(10): p. 1950-1957.DOI: <https://doi.org/10.2514/3.5487>.
17. Bradford, M.A., Azhari, M., *Inelastic local buckling of plates and plate assemblies using bubble functions*. Engineering Structures, 1995. **17**(2): p. 95-103.DOI: [https://doi.org/10.1016/0141-0296\(95\)92640-T](https://doi.org/10.1016/0141-0296(95)92640-T).
18. Ibearugbulem, O., Eziefula, U., Onwuka, D., *Inelastic stability analysis of uniaxially compressed flat rectangular isotropic CCSS plate*. International Journal of Applied Mechanics and Engineering, 2015. **20**(3): p. 637-645.DOI: <https://doi.org/10.1515/ijame-2015-0042>.
19. Ibearugbulem, O., Onwuka, D., Eziefula, U., *Inelastic buckling analysis of axially compressed thin CCCC plates using Taylor-Maclaurin displacement function*. Academic Research International, 2013. **4**(6): p. 594.
20. Onwuka, D., Eziefula, U., Ibearugbulem, O., *Inelastic Buckling of Rectangular Panel with a Simply Supported Edge and Three Clamped Edges under Uniaxial Loads*. International Journal of Applied Science and Engineering, 2016. **14**(1): p. 39-48.DOI: [https://doi.org/10.6703/IJASE.2016.14\(1\).39](https://doi.org/10.6703/IJASE.2016.14(1).39).
21. Eziefula, U., Onwuka, D., Ibearugbulem, O., *Work principle in inelastic buckling analysis of axially compressed rectangular plates*. World Journal of Engineering, 2017.DOI: <https://doi.org/10.1108/WJE-12-2016-0171>.
22. Shrivastava, S.C., *Inelastic buckling of plates including shear effects*. International Journal of Solids and Structures, 1979. **15**(7): p. 567-575.DOI: [https://doi.org/10.1016/0020-7683\(79\)90084-2](https://doi.org/10.1016/0020-7683(79)90084-2).

23. Guran, A., Rimrott, F.P.J., *Application of funicular polygon method to inelastic buckling analysis of plates*. Computer Methods in Applied Mechanics and Engineering, 1989. **76**(2): p. 157-170.DOI: [https://doi.org/10.1016/0045-7825\(89\)90093-5](https://doi.org/10.1016/0045-7825(89)90093-5).
24. Lau, S.C.W., Hancock, G.J., *Inelastic buckling analyses of beams, columns and plates using the spline finite strip method*. Thin-Walled Structures, 1989. **7**(3): p. 213-238.DOI: [https://doi.org/10.1016/0263-8231\(89\)90026-8](https://doi.org/10.1016/0263-8231(89)90026-8).
25. Rio, G., *Inelastic buckling of plate*. Archives of Mechanics, 1992. **44**(1): p. 105-116.
26. Azhari, M., Bradford, M.A., *Inelastic initial local buckling of plates with and without residual stresses*. Engineering Structures, 1993. **15**(1): p. 31-39.DOI: [https://doi.org/10.1016/0141-0296\(93\)90014-U](https://doi.org/10.1016/0141-0296(93)90014-U).
27. Wang, C.M., Xiang, Y., Chakrabarty, J., *Elastic/plastic buckling of thick plates*. International Journal of Solids and Structures, 2001. **38**(48): p. 8617-8640.DOI: [https://doi.org/10.1016/S0020-7683\(01\)00144-5](https://doi.org/10.1016/S0020-7683(01)00144-5).
28. Wang, C.M., Aung, T.M., *Plastic buckling analysis of thick plates using p-Ritz method*. International Journal of Solids and Structures, 2007. **44**(18): p. 6239-6255.DOI: <https://doi.org/10.1016/j.ijsolstr.2007.02.026>.
29. Lotfi, S., Azhari, M., Heidarpour, A., *Inelastic initial local buckling of skew thin thickness-tapered plates with and without intermediate supports using the isoparametric spline finite strip method*. Thin-Walled Structures, 2011. **49**(11): p. 1475-1482.DOI: <https://doi.org/10.1016/j.tws.2011.07.013>.
30. Zhang, W., Wang, X., *Elastoplastic buckling analysis of thick rectangular plates by using the differential quadrature method*. Computers & Mathematics with Applications, 2011. **61**(1): p. 44-61.DOI: <https://doi.org/10.1016/j.camwa.2010.10.028>.
31. Kasaeian, S., Azhari, M., Heidarpour, A., Hajiannia, A., *Inelastic local buckling of curved plates with or without thickness-tapered sections using finite strip method*. International Journal of Steel Structures, 2012. **12**(3): p. 427-442.DOI: <https://doi.org/10.1007/s13296-012-3011-9>.
32. Jaberzadeh, E., Azhari, M., Boroomand, B., *Inelastic buckling of skew and rhombic thin thickness-tapered plates with and without intermediate supports using the element-free Galerkin method*. Applied Mathematical Modelling, 2013. **37**(10): p. 6838-6854.DOI: <https://doi.org/10.1016/j.apm.2013.01.055>.
33. Kadkhodayan, M., Maarefdoust, M., *Elastic/plastic buckling of isotropic thin plates subjected to uniform and linearly varying in-plane loading using incremental and deformation theories*. Aerospace Science and Technology, 2014. **32**(1): p. 66-83.DOI: <https://doi.org/10.1016/j.ast.2013.12.003>.
34. Maarefdoust, M., Kadkhodayan, M., *Elastoplastic buckling analysis of rectangular thick plates by incremental and deformation theories of plasticity*. Proceedings of the Institution of Mechanical Engineers, Part G: Journal of Aerospace Engineering, 2015. **229**(7): p. 1280-1299.DOI: <https://doi.org/10.1177/0954410014550047>.
35. Maarefdoust, M., Kadkhodayan, M., *Elastic/plastic buckling analysis of skew plates under in-plane shear loading with incremental and deformation theories of plasticity by GDQ method*. Journal of the Brazilian Society of Mechanical Sciences and Engineering, 2015. **37**(2): p. 761-776.DOI: <https://doi.org/10.1007/s40430-014-0203-6>.
36. Gerard, G., Wildhorn, S., *A study of Poisson's ratio in the yield region*. 1952, NACA, Technical Note, No. 2561.

37. Ramberg, W., Osgood, W., *Description of stress-strain curves by three parameters*. 1943, NACA, Technical Note, No. 902.
38. Durban, D., *Plastic Buckling of Rectangular Plates Under Biaxial Loading*, in *Studies in Applied Mechanics*, I. Elishakoff, et al., Editors. 1988, Elsevier. p. 183-194.DOI: <https://doi.org/10.1016/B978-0-444-70474-0.50013-6>.
39. Ore, E., Durban, D., *Elastoplastic Buckling of Annular Plates in Pure Shear*. Journal of Applied Mechanics, 1989. **56**(3): p. 644-651.DOI: <https://doi.org/10.1115/1.3176141>.
40. Durban, D., Zuckerman, Z., *Elastoplastic buckling of rectangular plates in biaxial compression/tension*. International Journal of Mechanical Sciences, 1999. **41**(7): p. 751-765.DOI: [https://doi.org/10.1016/S0020-7403\(98\)00055-1](https://doi.org/10.1016/S0020-7403(98)00055-1).
41. Betten, J., Shin, C.H., *Elastic-plastic buckling analysis of rectangular plates subjected to biaxial loads*. Forschung im Ingenieurwesen, 2000. **65**(9): p. 273-278.DOI: <https://doi.org/10.1007/s100109900023>.
42. Kosel, F., Bremec, B., *Elastoplastic buckling of circular annular plates under uniform in-plane loading*. Thin-Walled Structures, 2004. **42**(1): p. 101-117.DOI: [https://doi.org/10.1016/S0263-8231\(03\)00126-5](https://doi.org/10.1016/S0263-8231(03)00126-5).
43. Wang, X., Huang, J., *Elastoplastic buckling analyses of rectangular plates under biaxial loadings by the differential quadrature method*. Thin-Walled Structures, 2009. **47**(1): p. 14-20.DOI: <https://doi.org/10.1016/j.tws.2008.04.006>.
44. Ahmed, M.Z., DaDeppo, D.A., *Stress distribution and buckling stress of plates including edge contact-frictional force effects*. International Journal of Solids and Structures, 1994. **31**(14): p. 1967-1979.DOI: [https://doi.org/10.1016/0020-7683\(94\)90202-X](https://doi.org/10.1016/0020-7683(94)90202-X).
45. Gjelsvik, A., Lin, G., *Plastic buckling of plates with edge frictional shear effects*. Journal of engineering mechanics, 1987. **113**(7): p. 953-964.DOI: [https://doi.org/10.1061/\(ASCE\)0733-9399\(1987\)113:7\(953\)](https://doi.org/10.1061/(ASCE)0733-9399(1987)113:7(953)).
46. Yao, Z., Rasmussen, K.J.R., *Inelastic local buckling behaviour of perforated plates and sections under compression*. Thin-Walled Structures, 2012. **61**: p. 49-70.DOI: <https://doi.org/10.1016/j.tws.2012.07.002>.
47. Azhari, M., Saadatpour, M.M., Bradford, M.A., *Inelastic local buckling of flat, thin-walled structures containing thickness-tapered plates*. Thin-Walled Structures, 2004. **42**(3): p. 351-368.DOI: <https://doi.org/10.1016/j.tws.2003.09.002>.
48. Samadi Dinani, A., Azhari, M., Sarrami Foroushani, S., *Elastic and Inelastic Buckling Analysis of Thick Isotropic and Laminated Plates Using Finite Layer Method* Civil Engineering Research Journal, 2017. **2**(4).DOI: <https://doi.org/10.19080/CERJ.2017.02.555593>.
49. Alinia, M.M., Gheitasi, A., Erfani, S., *Plastic shear buckling of unstiffened stocky plates*. Journal of Constructional Steel Research, 2009. **65**(8): p. 1631-1643.DOI: <https://doi.org/10.1016/j.jcsr.2009.04.001>.
50. Alinia, M.M., Soltanieh, G., Amani, M., *Inelastic buckling behavior of stocky plates under interactive shear and in-plane bending*. Thin-Walled Structures, 2012. **55**: p. 76-84.DOI: <https://doi.org/10.1016/j.tws.2012.03.007>.
51. Smith, S.T., Bradford, M., Oehlers, D.J., *Inelastic buckling of rectangular steel plates using a Rayleigh-Ritz method*. International Journal of Structural Stability and Dynamics, 2003. **3**(04): p. 503-521.DOI: <https://doi.org/10.1142/S021945540300102>.

52. Uenoya, M., Redwood, R.G., *Elasto-plastic shear buckling of square plates with circular holes*. Computers & Structures, 1978. **8**(2): p. 291-300.DOI: [https://doi.org/10.1016/0045-7949\(78\)90036-6](https://doi.org/10.1016/0045-7949(78)90036-6).
53. Wang, C., Aung, T.M., Kitipornchai, S., Xiang, Y., *Plastic-buckling of rectangular plates under combined uniaxial and shear stresses*. Journal of engineering mechanics, 2009. **135**(8): p. 892-895.DOI: [https://doi.org/10.1061/\(ASCE\)0733-9399\(2009\)135:8\(892\)](https://doi.org/10.1061/(ASCE)0733-9399(2009)135:8(892)).
54. Green, A.E., *Double Fourier series and boundary value problems*. Mathematical Proceedings of the Cambridge Philosophical Society, 1944. **40**(3): p. 222-228.DOI: <https://doi.org/10.1017/S0305004100018375>.
55. Kennedy, J.B., Prabhakara, M.K., *Buckling of Simply Supported Orthotropic Skew Plates*. Aeronautical Quarterly, 1978. **29**(3): p. 161-174.DOI: <https://doi.org/10.1017/S0001925900008428>.
56. Li, R., Zhong, Y., Tian, B., Du, J., *Exact bending solutions of orthotropic rectangular cantilever thin plates subjected to arbitrary loads*. International Applied Mechanics, 2011. **47**(1): p. 107-119.DOI: <https://doi.org/10.1007/s10778-011-0448-z>.
57. Li, R., Zhong, Y., Tian, B., Liu, Y., *On the finite integral transform method for exact bending solutions of fully clamped orthotropic rectangular thin plates*. Applied Mathematics Letters, 2009. **22**(12): p. 1821-1827.DOI: <https://doi.org/10.1016/j.aml.2009.07.003>.
58. Tian, B., Li, R., Zhong, Y., *Integral transform solutions to the bending problems of moderately thick rectangular plates with all edges free resting on elastic foundations*. Applied Mathematical Modelling, 2015. **39**(1): p. 128-136.DOI: <https://doi.org/10.1016/j.apm.2014.05.012>.
59. Tian, B., Zhong, Y., Li, R., *Analytic bending solutions of rectangular cantilever thin plates*. Archives of Civil and Mechanical Engineering, 2011. **11**(4): p. 1043-1052.DOI: [https://doi.org/10.1016/S1644-9665\(12\)60094-6](https://doi.org/10.1016/S1644-9665(12)60094-6).
60. Zhang, S., Xu, L., *Bending of rectangular orthotropic thin plates with rotationally restrained edges: A finite integral transform solution*. Applied Mathematical Modelling, 2017. **46**: p. 48-62.DOI: <https://doi.org/10.1016/j.apm.2017.01.053>.
61. Guerrero, J.S.P., Cotta, R.M., *Integral transform solution for the lid-driven cavity flow problem in streamfunction-only formulation*. International Journal for Numerical Methods in Fluids, 1992. **15**(4): p. 399-409.DOI: <https://doi.org/10.1002/flid.1650150403>.
62. An, C., Gu, J.-J., Su, J. *Integral transform solution of bending problem of clamped orthotropic rectangular plates*. in *International Conference on Mathematics and Computational Methods Applied to Nuclear Science and Engineering (M & C)*. 2011. Rio de Janeiro, RJ, Brazil: American Nuclear Society (ANS).
63. Ullah, S., Zhong, Y., Zhang, J., *Analytical buckling solutions of rectangular thin plates by straightforward generalized integral transform method*. International Journal of Mechanical Sciences, 2019. **152**: p. 535-544.DOI: <https://doi.org/10.1016/j.ijmecsci.2019.01.025>.
64. Zhang, J., Zhou, C., Ullah, S., Zhong, Y., Li, R., *Two-dimensional generalized finite integral transform method for new analytic bending solutions of orthotropic rectangular thin foundation plates*. Applied Mathematics Letters, 2019. **92**: p. 8-14.DOI: <https://doi.org/10.1016/j.aml.2018.12.019>.

65. He, Y., An, C., Su, J., *Generalized integral transform solution for free vibration of orthotropic rectangular plates with free edges*. Journal of the Brazilian Society of Mechanical Sciences and Engineering, 2020. **42**(4): p. 183.DOI: 10.1007/s40430-020-2271-0.
66. *Python Language Reference*. 2019, Python Software Foundation. <http://www.python.org>.
67. Pride, R., Heimerl, G., *Plastic buckling of simply supported compressed plates*. 1948, NACA, Technical Note, No. 1817.

Declaration

- **Funding** (information that explains whether and by whom the research was supported)

Not applicable

- **Conflicts of interest/Competing interests** (include appropriate disclosures)

There is no conflict of interest.

- **Availability of data and material** (data transparency)

Not applicable

- **Code availability** (software application or custom code)

Not applicable